iScience

CellPress
OPEN ACCESS

Article

Topiramate suppresses peri-infarct spreading depolarization and improves outcomes in a rat model of photothrombotic stroke

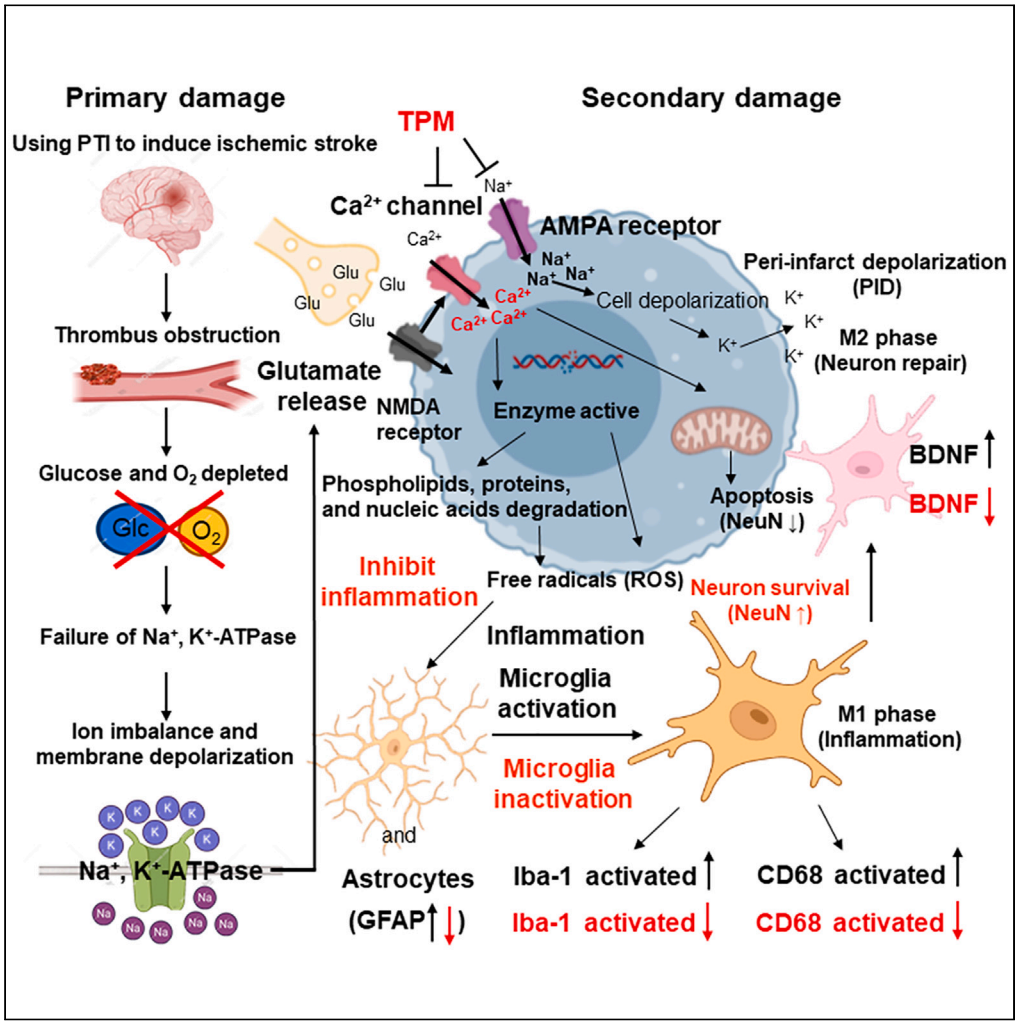

Yuhling Wang, Shaoyu Yen, Yen-Yu Ian Shih, ..., Li-Tzong Chen, Hsi Chen, Lun-De Liao

ldliao@nhri.edu.tw

Highlights

ECoG-LSCI reveals the neurovascular function of topiramate in stroke treatment

Topiramate administration significantly restored somatosensory evoked potentials

Topiramate increases apoptosis and neuronal survival in stroke treatment

Topiramate attenuates the effects of PID and reduces infarct volume

Wang et al., iScience 27, 110033
June 21, 2024
https://doi.org/10.1016/j.isci.2024.110033

iScience

CellPress
OPEN ACCESS

Article

Topiramate suppresses peri-infarct spreading depolarization and improves outcomes in a rat model of photothrombotic stroke

Yuhling Wang,[1,7] Shaoyu Yen,[1] Yen-Yu Ian Shih,[2,3,4] Chien-Wen Lai,[1] Yu-Lin Chen,[1] Li-Tzong Chen,[5,6] Hsi Chen,[1] and Lun-De Liao[1,8,*]

SUMMARY

Ischemic stroke can cause depolarized brain waves, termed peri-infarct depolarization (PID). Here, we evaluated whether topiramate, a neuroprotective drug used to treat epilepsy and alleviate migraine, has the potential to reduce PID. We employed a rat model of photothrombotic ischemia that can reliably and reproducibly induce PID and developed a combined electrocorticography-laser speckle contrast imaging (ECoG-LSCI) platform to monitor neuronal activity and cerebral blood flow (CBF) simultaneously. Topiramate administration after photothrombotic ischemia did not rescue CBF but significantly restored somatosensory evoked potentials in the forelimb area of the primary somatosensory cortex. Moreover, infarct volume was investigated by 2,3,5-triphenyltetrazolium chloride (TTC) staining, and neuronal survival was evaluated by Nissl staining. Mechanistically, the levels of inflammatory markers, such as ED1 (CD68), Iba-1, and GFAP, decreased significantly after topiramate administration, as did BDNF expression, while the expression of NeuN and Bcl-2/Bax increased, which is indicative of reduced inflammation and improved neuroprotection.

INTRODUCTION

Stroke is the second leading cause of death worldwide.[1] At present, the only clinical drug approved by the Food and Drug Administration (FDA) for the treatment of acute ischemic stroke is recombinant tissue plasminogen activator (rtPA), a fibrin-specific activator that can convert plasminogen into plasmin to dissolve thrombi and is usually applied within 4.5 h of stroke onset.[2] Neuroprotective strategies that have the potential to improve the management of acute stroke can offer considerable public health benefits.[3]

One common pathological feature among acute stroke, epilepsy, traumatic brain injury (TBI), and subarachnoid hemorrhage (SAH) is the sudden imbalance of the neuronal transmembrane ionic gradient and the resulting depolarization waves, commonly known as cortical spreading depression (CSD).[4] According to a canonical model, CSD is caused by the increasing accumulation of potassium ions outside cells. This subsequent inflow of potassium ions can trigger depolarization followed by a transient increase in cerebral blood flow (CBF), local tissue oxygen tension, and metabolism.[5] CSD typically spreads across the gray matter of the brain at a speed of 2–6 mm/min, which is consistent across rodents, nonhuman primates, and humans.[4,6] Importantly, in a normally perfused, healthy brain, CSD typically does not cause notable tissue damage; however, it leads to a severe shortage of adenosine triphosphate (ATP) and can exacerbate preexisting brain tissue damage.[7] In the case of stroke, such events often initiate from the peri-infarct areas and are thus termed peri-infarct depolarization (PID).[8] It has also been shown that the flow polarity is different in the peri-infarct area and normal tissue after stroke, and the flow velocity is slower in the penumbra area than in the normal cortical area.[9] Due to the loss of oxygen, glucose, and nutrients in the ischemic region, sodium-potassium pumps fail to maintain ion balance due to the lack of ATP, which leads to depolarization, increased cellular permeability,[3] excessive glutamate release, and excitotoxicity.[2,9,10] These changes, in turn, stimulate the Na^+/Ca^{2+} channel coupled with the α-amino-3-hydroxy-5-methyl-4-isoxazole propionic acid receptor (AMPAR), the *N*-methyl-D-aspartate receptor (NMDAR) and the kainic acid receptor (KAR), further depolarizing the membrane of postsynaptic neurons and opening the membrane potential-sensitive voltage-gated sodium (Na^+) channel (VGNC) and voltage-gated calcium channel (VGCC).[11] These channels permit more Ca^{2+} and Na^+ to flow into the cell, causing intracellular calcium overload and further impairing the generation of ATP from the mitochondria.[12] It follows that high levels of intracellular Ca^{2+} and the activation of endonucleases and free radicals can promote the decomposition of phospholipids, proteins, and nucleic acids and trigger the apoptosis cascade.[11]

[1]Institute of Biomedical Engineering and Nanomedicine, National Health Research Institutes, 35, Keyan Road, Zhunan Town, Miaoli County 350, Taiwan
[2]Center for Animal MRI, University of North Carolina at Chapel Hill, Chapel Hill, NC 27599, USA
[3]Biomedical Research Imaging Center, University of North Carolina at Chapel Hill, Chapel Hill, NC 27599, USA
[4]Department of Neurology, University of North Carolina at Chapel Hill, Chapel Hill, NC 27599, USA
[5]Kaohsiung Medical University Hospital, Kaohsiung Medical University, No. 100, Shih-Chuan 1st Road, Sanmin District, Kaohsiung City 80708, Taiwan
[6]National Institute of Cancer Research, National Health Research Institutes, No. 35, Keyan Road, Zhunan Township, Miaoli County 350, Taiwan
[7]Department of Electrical Engineering, National United University, NO.2, Lien Da, Nan Shih Li, Miao-Li 36063, Taiwan
[8]Lead contact
*Correspondence: ldliao@nhri.edu.tw
https://doi.org/10.1016/j.isci.2024.110033

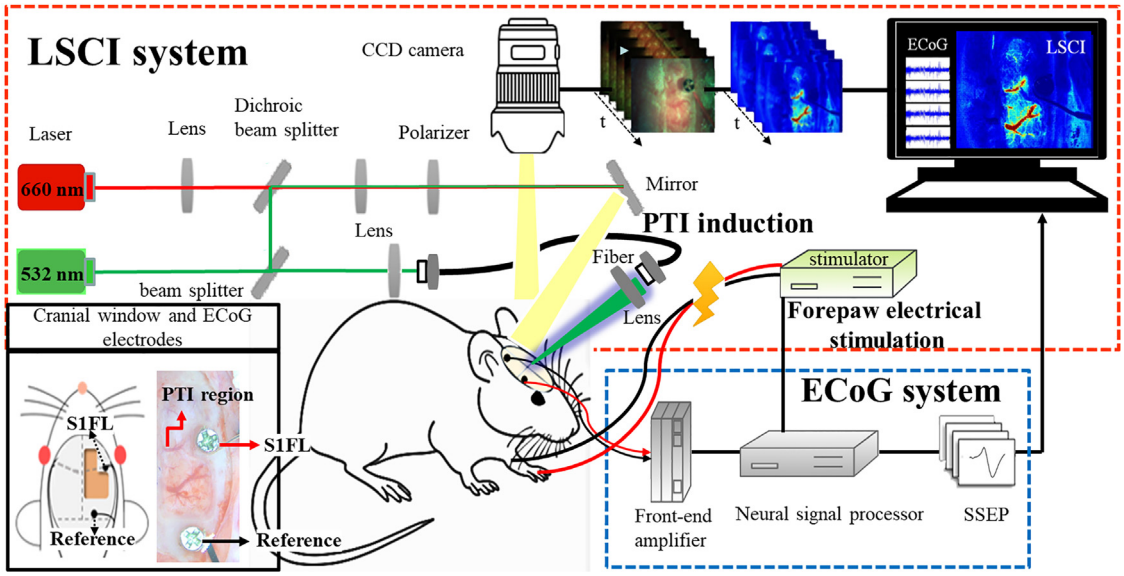

Figure 1. Diagram of the ECoG-LSCI system and experimental setup

The ECoG-LSCI system was used to investigate neurovascular function and cortical activity in rats. The setup included an ECoG recording system, an LSCI imaging system, a laser to induce photothrombotic ischemia in the cortex, and a forepaw electrical stimulation system. The animal was placed on the stereotaxic table, and an infrared warming lamp was used to maintain the animal's body temperature at 38°C. A screw electrode was fixed in the S1FL area of the brain, and another reference electrode was inserted 3 mm to the right of lambda to receive the ECoG signal and amplified via a front-end amplifier. A craniotomy window was created in the S1FL region (lower left image), and the cortical region of interest was illuminated with a CW 660 nm laser. The CCD camera was placed above the craniotomy window to collect speckle pattern images. Rats were injected with Rose Bengal (diluted to 10 mg/mL in saline and administered at 0.2 mL/100 g body weight) via the tail vein, and then the laser was focused on selected MCA arterioles in the S1FL region for 30 min to induce photothrombotic ischemia (PTI). Then, the DS3 stimulator was used to trigger contralateral peripheral electrical stimulation.

There is emerging evidence that the number of PIDs is not significantly associated with the final infarct size[4] but instead is significantly correlated with the volume of the ischemic penumbra.[4] As CSDs appear only in the presence of the ischemic penumbra and can exacerbate tissue damage,[13] it is plausible that suppressing CSDs during acute stroke can lead to reduced excitotoxicity and improved outcomes. One candidate drug used for this purpose is topiramate, an FDA-approved agent for the treatment of migraine and epilepsy known to inhibit VGNCs, VGCCs, and AMPARs.[14] Specifically, topiramate can effectively reduce the inhibition of cortical diffusion in the context of migraine[15] and block VGNCs to ameliorate epilepsy.[16] In animal models, topiramate has been shown to enhance chloride ion influx through the γ-amino-butyric acid (GABA) receptor, effectively reduce excitotoxicity in neurons, and antagonize KAR and AMPAR to promote stable membrane currents in neurons and glial cells.[14] Cellular patch-clamp studies have shown that the suppression of L-type VGCC currents by topiramate also contributes to its ability to reduce neuronal excitability.[14] While topiramate has been shown to reduce the frequency of CSD in migraine patients,[17] its potential efficacy in suppressing PIDs has yet to be explored.

Understanding the putative influence of topiramate on PIDs as well as the relevant neuronal activity and corresponding CBF supplies requires dynamic imaging of both metrics *in vivo*. Here, we established a novel electrocorticography-laser speckle contrast imaging (ECoG-LSCI) platform capable of assessing changes in neurovascular coupling across space and time. The benefit of ECoG over electroencephalography (EEG) is the reduced interference from the meninges, cerebral tissue fluid, and cranium. While ECoG detects population neuronal activity and has high temporal resolution, it has limited spatial resolution and cannot provide information on CBF.[18] This limitation was addressed by the inclusion of the LSCI technique, which allows precise monitoring of the CBF throughout the progression of acute stroke with high spatiotemporal resolution.[15,16] Using this novel platform, we first examined the ability of 1 M and 4 M KCl to induce CSDs and then evaluated PIDs via a photothrombotic model that is known to reliably and reproducibly induce PIDs.[4] We report the influences of topiramate on CSDs and PIDs, as well as the final infarct volume, as assessed by 2,3,5-triphenyltetrazolium chloride (TTC) staining. Moreover, we determine the severity of the morphological changes in the blood cells using Nissl staining. Our results elucidate the possibility of using PID-suppressing, neuroprotective agents for acute stroke management in the future.

RESULTS

ECoG-LSCI to measure KCl-induced CSD

First, to confirm the feasibility of using ECoG-LSCI (Figure 1), we used 1 M and 4 M KCl to determine whether the instrument could reliably detect CSDs (Figure 2). The device was also used to detect PID induced by electrical stimulation around photothrombotic ischemia (Figure 3).

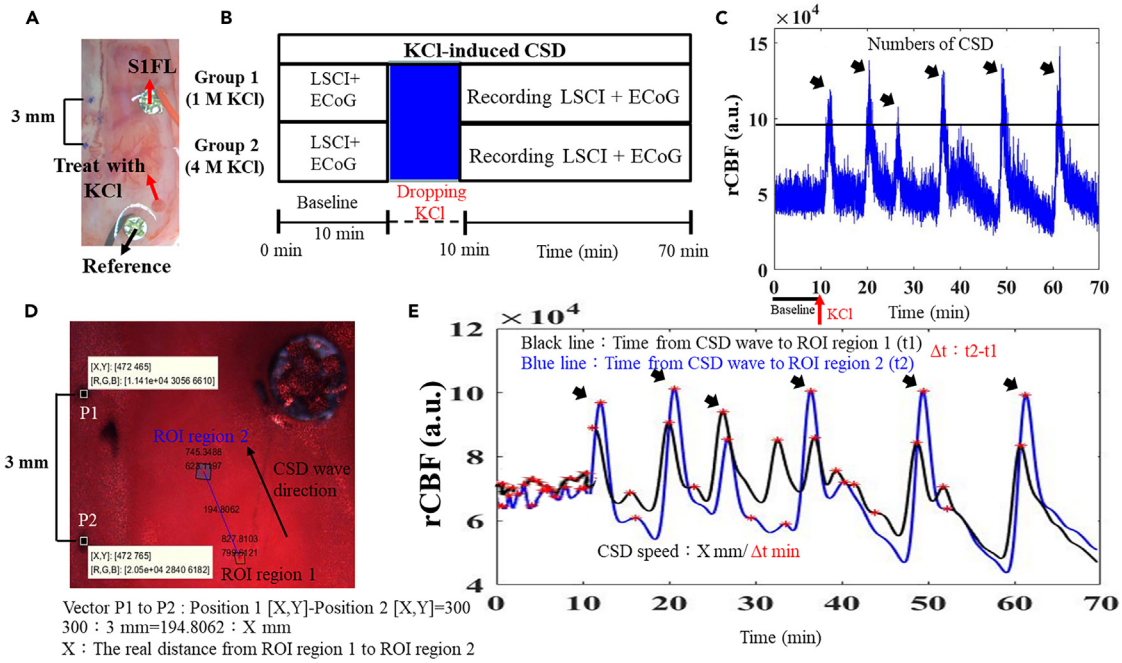

Figure 2. Experimental protocol for KCl induction of CSD and the method for calculating CSD speed

(A) CCD image of a rat brain. Two points were marked with a 3 mm distance between them for use as a scale for calculating CSD speed. The electrodes (screws) on the upper right were used to collect the ECoG signals. A hole was created in the bottom right of the skull, and KCl was added to induce CSD.

(B) Before adding KCl, the LSCI and ECoG signals were recorded for 10 min to establish a baseline and for 60 min after 1 M and 4 M KCl were used to induce CSD.

(C) Plot of CBF vs. time. To count the number of CSDs, a threshold level was determined. When the CBF exceeded the threshold, it was considered a CSD.

(D) MATLAB was used to analyze all images, and two ROIs were circled in the image to obtain the CSD speed. By comparing the difference in time between the peaks in the CBF appearing in the two ROIs and calculating the distance between the two ROIs, the CSD speed (in mm/min) was computed.

(E) Changes in CBF vs. time for both ROIs plotted in the same window. The time difference between the peaks in the two ROIs (Δt) was used to calculate the CSD speed as X mm/Δt min.

We were able to observe CSDs as transient suppression of ECoG signals (Figures 4A and 4D) and increases in the CBF (Figures 4B and 4E). Figures 4C and 4F show the spatial propagation of a CSD event imaged at 25 s intervals (Video S1).

Figures 5A and 5B show the ROIs drawn to calculate the speed of CSD propagation in the two groups of subjects. The CBFs from the two ROIs were plotted (Figures 5C and 5D), and the time difference between the peaks was used to calculate the speed of CSD propagation. KCl (1 M) induced 1.20 ± 0.20 CSDs, while KCl (4 M) induced 4.80 ± 0.58 CSDs, as shown in Figure 5E. The number of CSDs induced by 4 M KCl was significantly greater than that induced by 1 M KCl ($p < 0.05$). The CSD speed did not differ according to KCl concentration (1 M KCl: 4.03 ± 0.55 mm/min, 4 M KCl: 3.70 ± 0.34 mm/min; Figure 5F).

Topiramate has no effect on restoring CBF following photothrombotic ischemia

Next, we examined the LSCI data to evaluate the effect of topiramate on CBF after photothrombotic ischemia. Representative bright field and LSCI contrast images before and after sham or ischemia induction in the control, untreated, and topiramate-treated groups are shown in Figure 6A. In the control group, the normalized CBF values at 0, 1, 2, and 3 h after the sham procedure were 106.80% ± 5.95, 95.36% ± 11.75, 101.61% ± 11.24 and 100.13% ± 13.82, respectively (Figure 6B), and these values were not significantly different from those at baseline, which was set to 100%. In the untreated photothrombotic ischemia group, the CBF values were 8.50% ± 0.35, 8.76% ± 0.83, 7.91% ± 0.63 and 7.70% ± 0.78, respectively (Figure 6C). In the topiramate-treated photothrombotic ischemia group, the CBF values were 17.54% ± 1.72, 15.13% ± 1.15, 13.72% ± 1.15 and 14.77% ± 1.0, respectively (Figure 6D). The CBF after the induction of ischemia was significantly lower than that before ischemia in both the treated and untreated groups ($p < 0.05$). Based on these results, topiramate did not affect CBF or thrombus formation during photothrombotic ischemia.

Topiramate improves somatosensory evoked potentials following photothrombotic ischemia

We used ECoG to record the forepaw stimulus-evoked SSEPs in the S1FL area of the rat brain as an indicator of neural function. The SSEP peak-to-peak amplitude before any procedures were performed was defined as the baseline (100%), and the SSEPs were recorded every hour after sham or photothrombotic ischemia induction. Figures 7A–7C show representative SSEP traces. In the control group, the amplitudes at 0, 1, 2,

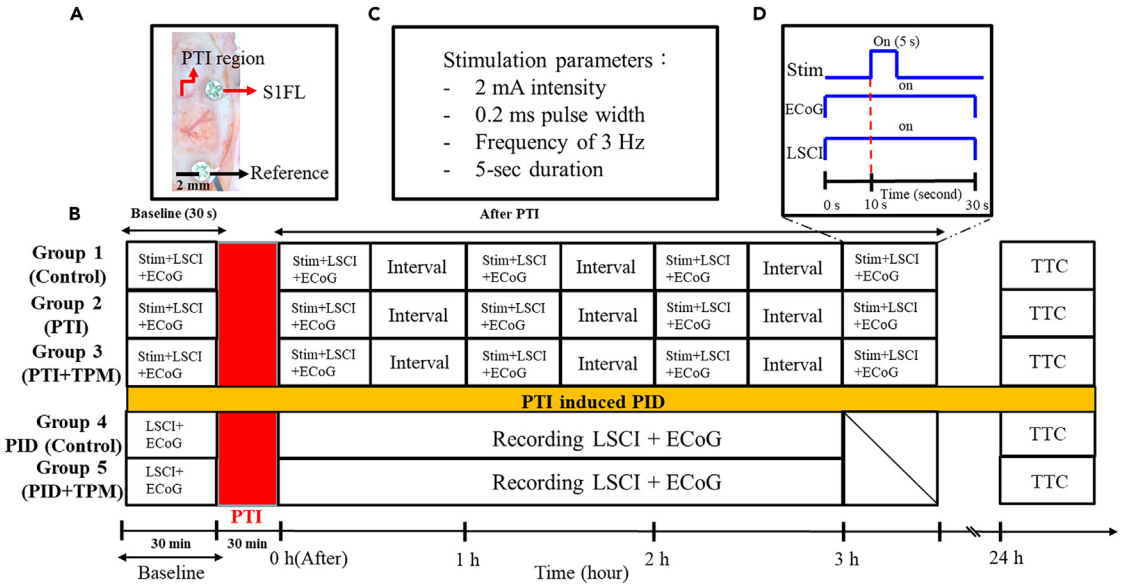

Figure 3. Protocol for peripheral stimulation and ECoG-LSCI recording and monitoring of photothrombotic ischemia-induced PID

(A) The cranial window illustrates the placement of an epidural electrode in the S1FL area (ML: +4 mm/AP: +1 mm) and a reference electrode approximately 3 mm to the right of lambda to record the ECoG signal. Scale bar = 2 mm.

(B) The SSEPs before and every 1 h after photothrombotic ischemia (PTI) were compared between Groups 1–3 to examine the effect of topiramate treatment on the recovery of neural function. TTC staining was performed 24 h after the induction of photothrombotic ischemia. The data from groups 4 and 5 were compared to observe the progression of photothrombotic ischemia-induced PID and the effect of topiramate treatment. The LSCI and ECoG signals were recorded before photothrombotic ischemia as a baseline and for 3 h after the induction of photothrombotic ischemia, followed by TTC staining 24 h after photothrombotic ischemia initiation.

(C) The sensory electrical stimulation parameters were an amplitude of 2 mA, pulse width of 0.2 ms, frequency of 3 Hz, and duration of 5 s.

(D) LSCI and ECoG signals were recorded for 60 s, and electrical stimulation was initiated for 5 s at the 10th second.

and 3 h were 96.56% ± 5.48, 97.21% ± 4.71, 95.80% ± 4.68 and 97.57% ± 3.88, respectively. In the untreated photothrombotic ischemia group, the amplitudes were 13.98% ± 0.73, 12.70% ± 0.85, 14.06% ± 0.68 and 14.22% ± 1.57, respectively. In the topiramate-treated photothrombotic ischemia group, the amplitudes were 9.10% ± 1.47, 28.98% ± 6.69, 58.24% ± 5.38, and 77.25% ± 4.10, respectively (Figure 7D). Similar to the CBF results, the SSEP amplitudes at 0 h were significantly different only from baseline in the treated and untreated photothrombotic ischemia groups ($p < 0.05$). At 3 h, however, the SSEP amplitude in the untreated group remained significantly lower than the baseline level ($p < 0.05$), whereas the SSEP amplitude in the treated group returned to baseline. This finding demonstrated the potential neuroprotective effect of topiramate treatment.

Topiramate reduces the number of PIDs following photothrombotic ischemia

We then examined whether topiramate treatment can reduce the number of PIDs during ischemia. Figure 8A shows the ECoG signals recorded before, during, and after photothrombotic ischemia, where the signal amplitude decreased after the induction of ischemia. Figure 8B shows the simultaneously recorded change in CBF, where multiple PID events occurred after the induction of ischemia. As expected, PID spread outward from the ischemic core into the surrounding regions (Figure 8C). The ECoG-LSCI data obtained after photothrombotic ischemia and topiramate treatment are shown in Figures 8D–8F (Video S2). Topiramate treatment reversed the suppression of ECoG signals and reduced the number of PID events.

Figures 9A and 9B show the ROI placement from which the PID speed in the photothrombotic ischemia group and photothrombotic ischemia+topiramate administration group were calculated. Changes in the CBF in the two ROIs are shown in Figures 9C and 9D. The PID speeds were 4.8 ± 0.37 mm/min in the untreated group and 2.8 ± 0.37 mm/min in the topiramate-treated group (Figure 9E), while the PID speeds were 4.14 ± 0.32 mm/min in the untreated group and 4.34 ± 0.33 mm/min in the topiramate-treated group (Figure 9F). Treatment with topiramate significantly reduced the number of PIDs ($p < 0.05$) but did not affect the PID speed.

Topiramate reduces the infarct volume following photothrombotic ischemia

To confirm the occurrence, size, and severity of brain damage caused by the photothrombotic ischemic stroke investigation system, we utilized two staining methods to evaluate ischemic lesions, as shown in Figure 10. First, TTC staining was used to assess ischemic damage. Figure 10A shows an example of a coronal brain section, where 0.0 mm was set as the center of ischemia induction. In the control group, the

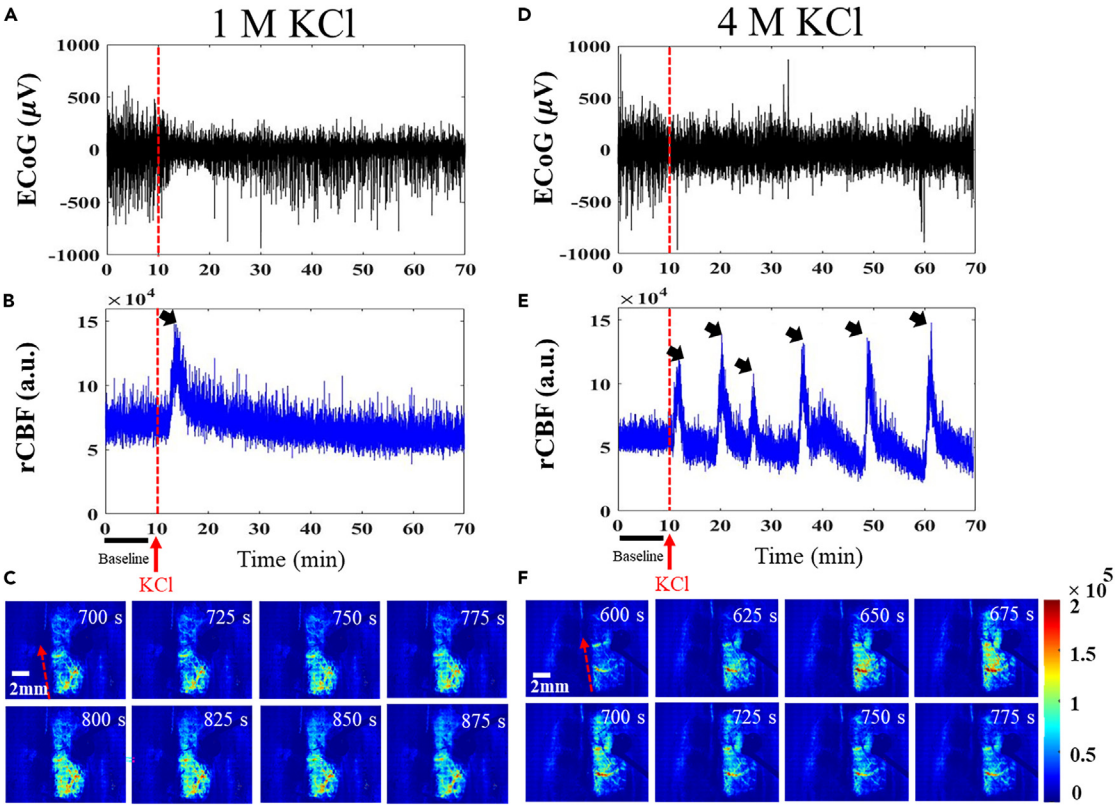

Figure 4. Neurovascular function observed using ECoG-LSCI after the administration of different concentrations of KCl

Changes in the ECoG signal (A) and CBF (B) during CSD induction with 1 M KCl. The CBF peaks occurred simultaneously with electrical inhibition of the ECoG signal. There was 1 occurrence of CSD (black arrow).

(C) Example images mapping the CBF on the cortical surface from 700 to 875 s taken at 25 s intervals (Video S1). KCl was applied near the bottom of the image, and the direction of CSD propagation is indicated by the red arrow. Changes in the ECoG signal (D) and CBF (E) during CSD induction with 4 M KCl. The CBF peaks occurred simultaneously with the electrical inhibition of the ECoG signal. There were 6 occurrences of CSD (black arrows).

(F) Example images mapping the CBF on the cortical surface from 600 to 775 s taken in 25 s intervals (Video S1). The red dotted arrow represents the direction of CSD propagation.

unaffected healthy cortex appeared red after TTC staining, whereas the infarct area appeared white. The quantification of infarct volume is shown in Figure 10B. The infarct volume was greatest at approximately 0.0 mm and decreased outward from the center of ischemia induction. The infarct volume in the untreated photothrombotic ischemia group was 4.5% ± 0.1, which was significantly greater than that in the topiramate-treated photothrombotic ischemia group (2.8% ± 0.2) (Figure 10C; $p < 0.05$). Nissl staining revealed that the neurons in the control group exhibited a complete granular morphology. The plasma was densely stained by toluidine blue, indicating sufficient nutrient supply and active energy synthesis. However, the number of neurons in the prothrombotic ischemia (PTI) group was significantly reduced, and the neuronal morphology was irregular. The intracellular toluidine blue staining was also significantly reduced and diffuse. In the topiramate group, the neurons were preserved, but in reduced numbers (Figure 10D). Nissl-stained tissue showed pale degenerated neurons in ischemic areas, indicating that our photothrombotic ischemia-inducing system caused stroke.

Effect of topiramate on NeuN, BDNF, ED1 (CD68), Iba-1, GFAP, Bax and Bcl-2 following photothrombotic ischemia

Western blotting was used to compare the expression levels of NeuN, BDNF, ED1 (CD68), Iba-1, GFAP, Bcl-2, and Bax in the core, penumbra, and normal cortex of treated and untreated animals (Figure 11A). The normalized levels of NeuN (see STAR methods for details), a neuronal marker, in the ischemic core region were 2.61 ± 0.19 in the control group, 1.53 ± 0.08 in the untreated photothrombotic ischemia group, and 2.48 ± 0.20 in the topiramate-treated group (Figure 11B). These data suggested that there was significant neuronal loss following photothrombotic ischemia and that topiramate had a neuroprotective effect (both $p < 0.05$). Both ED1 (CD68) and Iba-1 are markers of macrophages. The ED1 (CD68) level in the ischemic core region was 0.54 ± 0.08 in the control group, 4.24 ± 0.63 in the untreated photothrombotic ischemia group, and 1.92 ± 0.49 in the topiramate-treated group. The ED1 (CD68) level in the penumbra region was 0.86 ± 0.18 in the control group, 2.29 ± 0.57 in the untreated photothrombotic ischemia group, and 1.21 ± 0.28 in the topiramate-treated group (Figure 11C). The

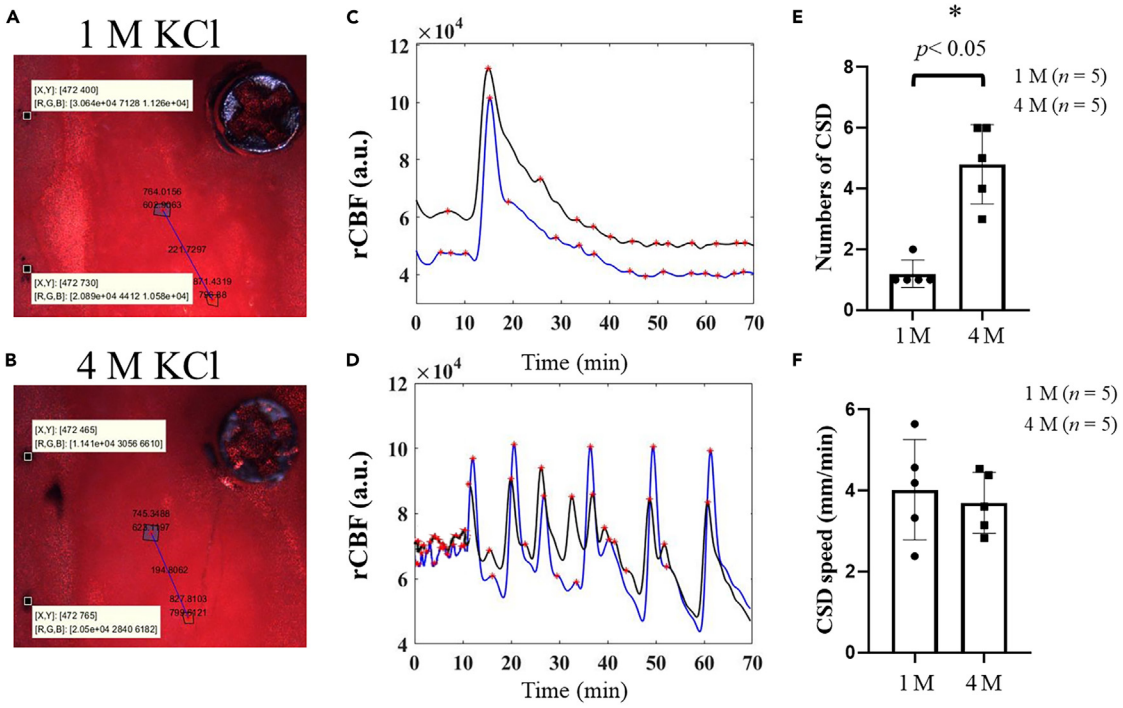

Figure 5. The number of CSD events was dependent on the KCl concentration, but there was no significant difference in speed

Representative images of the cortical surface of a rat treated with 1 M (A) and 4 M (B) KCl. The ROIs used to determine the CSD speed are shown.

(C and D) The numbers of CSDs and the time to reach 2 ROIs at different concentrations of KCl.

(E) With 1 M KCl, the CSD number was 1.2 ± 0.2, while the CSD number with 4 M KCl was 4.8 ± 0.58. After 4 M KCl stimulation, the number of CSDs was significantly greater than that after stimulation with 1 M KCl ($p < 0.05$).

(F) With 1 M KCl, the average CSD speed was 4.03 ± 0.55 mm/min, while the average CSD speed with 4 M KCl was 3.70 ± 0.34 mm/min. There was no significant difference in the CSD speed after treatment with different concentrations of KCl.

Iba-1 level in the core region was 0.33 ± 0.09 in the control group, 1.45 ± 0.27 in the untreated photothrombotic ischemia group, and 0.58 ± 0.15 in the topiramate-treated group (Figure 11D). The Iba-1 level in the penumbra region was 0.35 ± 0.09 in the control group, 1.06 ± 0.16 in the untreated photothrombotic ischemia group, and 0.63 ± 0.17 in the topiramate-treated group. These data suggested that the inflammation and macrophage recruitment to the core and penumbra regions that followed photothrombotic ischemia could be suppressed by topiramate ($p < 0.05$). After topiramate administration, ED1 (CD68) and Iba-1 expression was significantly decreased in both the ischemic core and penumbra regions (Figures 11C and 11D; $p < 0.05$).

GFAP is a glial cell marker that also indicates neuroinflammation. The GFAP level in the ischemic core region of the control group was 0.11 ± 0.02, and this value was 1.35 ± 0.19 in the untreated photothrombotic ischemia group and 0.62 ± 0.15 in the topiramate-treated group. In the penumbra region, GFAP level was 0.17 ± 0.06 in the control group, 1.06 ± 0.09 in the untreated photothrombotic ischemia group, and 0.73 ± 0.08 in the topiramate-treated group. In the distant cortex, the GFAP level was 0.11 ± 0.05 in the control group, 0.65 ± 0.08 in the untreated photothrombotic ischemia group, and 0.27 ± 0.07 in the topiramate-treated group. These results suggested that photothrombotic ischemia significantly increased the number of glial cells, which was suppressed by treatment with topiramate (Figure 11E; $p < 0.05$).

BDNF is an important protein that promotes neuron growth and repair. The BDNF level in the ischemic core region was 0.69 ± 0.16 in the control group, 1.67 ± 0.19 in the photothrombotic ischemia group, and 1.11 ± 0.08 in the topiramate-treated group. These results suggested significantly increased neuronal growth and repair after photothrombotic ischemia ($p < 0.05$) but not after topiramate treatment. No significant difference in BDNF expression was observed in the penumbra or distant cortex, as shown in Figure 11F.

The expression of the antiapoptotic protein Bcl-2 and the proapoptotic protein Bax was measured to gain insight into apoptotic signaling. Compared with that in the control group, the damage to the core area in the photothrombotic ischemia group caused significantly decreased Bcl-2 expression, while topiramate treatment significantly alleviated the decrease in Bcl-2 expression. The Bax content in the photothrombotic ischemia group was significantly greater than that in the control group. Moreover, topiramate treatment significantly improved the increase in the Bax content. The Bcl-2/Bax ratio in the core photothrombotic ischemia group (0.586 ± 0.08) was significantly lower than that in the topiramate-treated group (0.837 ± 0.08). Compared with this ratio in the topiramate-treated group, the penumbra photothrombotic ischemia group (0.520 ± 0.05) exhibited a significant decrease (0.749 ± 0.10) (Figure 11G; $p < 0.05$).

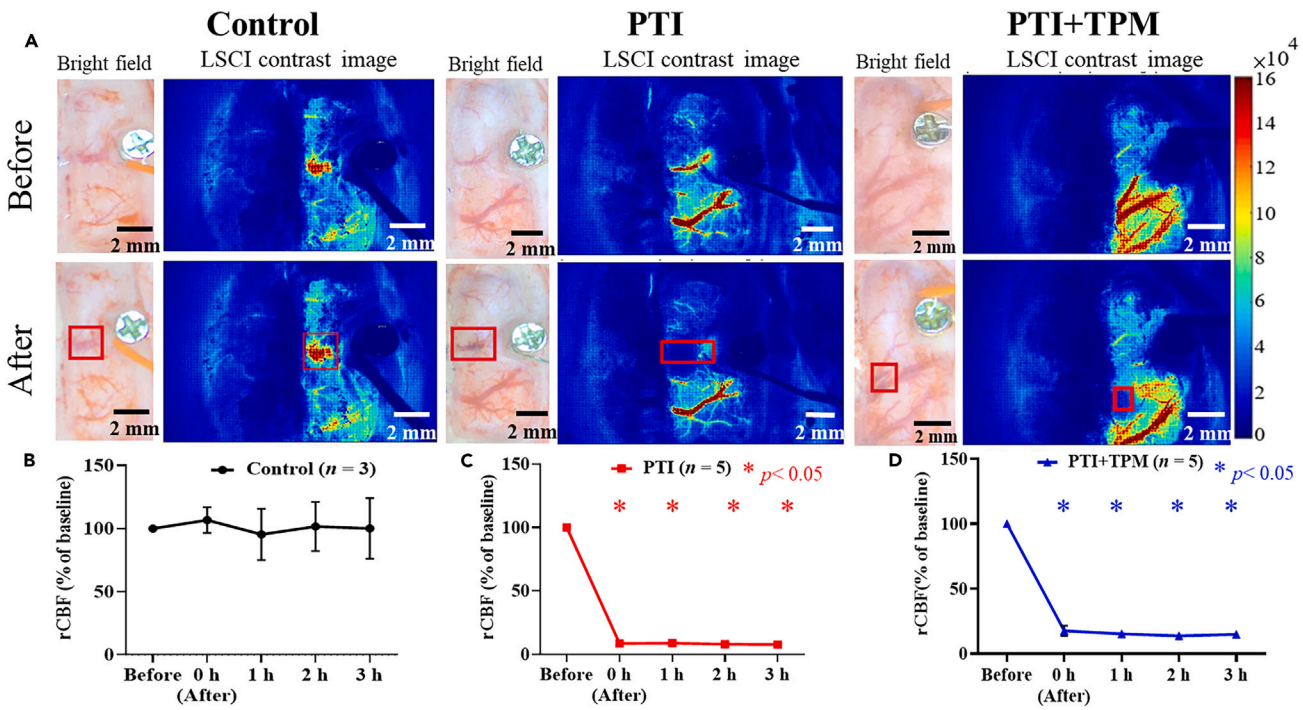

Figure 6. Topiramate has no effect on CBF recovery in photothrombotic ischemia

(A) Representative bright field and LSCI contrast images obtained before and after photothrombotic ischemia. In the photothrombotic ischemia groups, the absence of blood flow after the induction of ischemia was observed in the blood vessels, as indicated by the red rectangles.

(B) The CBF in the control group remained unchanged, indicating that it was not affected by photothrombotic ischemia. At 0 h, 1 h, 2 h, and 3 h, the CBF values were 106.80 ± 5.95%, 95.36 ± 11.75%, 101.61 ± 11.24%, and 100.13 ± 13.82% of the baseline, respectively.

(C) CBF in the photothrombotic ischemia group. At 0 h, 1 h, 2 h and 3 h, the CBF values were 8.50 ± 0.35%, 8.76 ± 0.83%, 7.91 ± 0.63% and 7.70 ± 0.78% of the baseline, respectively.

(D) Topiramate had no thrombolytic effect since the CBF was significantly lower after the induction of ischemia ($p < 0.05$). At 0 h, 1 h, 2 h, and 3 h, the CBF values were 17.54 ± 1.72%, 15.13 ± 1.15%, 13.72 ± 1.15%, and 14.77 ± 1.0% of the baseline, respectively.

DISCUSSION

CSD detection using ECoG-LSCI

Globally, stroke is one of the top three causes of mortality and the most frequent cause of permanent disability.[19] Multimodal recording tools are critically needed to examine the pathophysiological dynamics of stroke and the efficacy of treatment in research settings.[14] LSCI probes CBF information at high spatial and temporal resolution with a wide field of view[18,20,21] and has shown promising utility for stroke research.[22] Here, we coupled LSCI with ECoG to examine both vascular and neuronal activity changes *in vivo*. Using these complementary measures, we successfully detected KCl-induced CSDs with both electrophysiological and flow metrics (Figures 4 and 5). Although KCl is commonly used to induce CSDs,[4] it should be noted that the number of CSDs induced by KCl may vary according to the experimental settings, animal physiology, treatment times, and KCl concentrations.[23–25] In contrast, CSD velocity appears rather consistent – the values reported in this study are in agreement with previous findings,[4,23] ranging between 1.7 and 9.2 mm/min[7].

Influence of topiramate on photothrombotic ischemia

We used ECoG-LSCI to examine the neuroprotective effect and changes in CBF following photothrombotic ischemia. As expected, topiramate had no effect on blood flow restoration after thrombosis. Importantly, we found that SSEPs were restored by topiramate, suggesting its potential neuroprotective effect.

Thrombus formation after photothrombotic ischemia prevents the CBF from transporting nutrients such as oxygen and glucose.[2,10] As a consequence, neurons suffer from insufficient ATP derived via glycolysis, leading to a decrease in sodium-potassium pump function, ionic imbalance, and ultimately depolarization.[2,10] Moreover, this process releases a large amount of glutamate, which induces excitotoxicity and promotes the entry of sodium and calcium ions into cells, releasing potassium ions and triggering the spatial "spreading" of depolarization, which is often termed PID in the case of stroke.[2,10] Fu et al. showed that topiramate can inhibit calcium channels,[26] which reduces glutamate-induced excitatory signaling and enhances inhibitory signaling mediated by GABA.[10] Topiramate also blocks sodium channels and acts as a $GABA_A$ receptor antagonist, which suppresses the firing of action potentials.[27,28] These processes can stabilize cell membrane currents

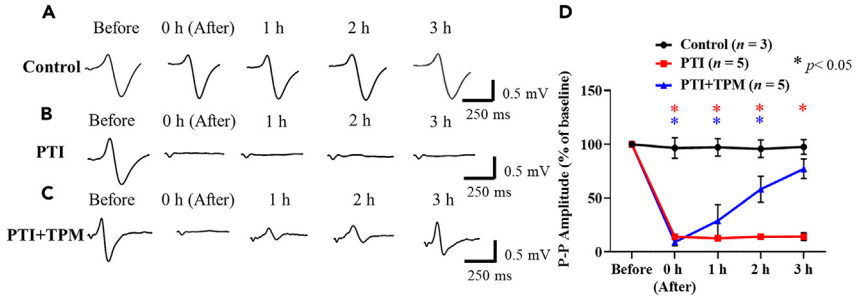

Figure 7. The neuroprotective effects of topiramate were evident in the SSEP measurements

(A) The average SSEPs before and after sham stroke in the control group did not change. The peak-to-peak (P-P) amplitudes at 0 h, 1 h, 2 h and 3 h were 96.56 ± 5.48%, 97.21 ± 4.71%, 95.80 ± 4.68% and 97.57 ± 3.88% of the baseline, respectively.

(B) The average SSEPs before and after stroke in the untreated photothrombotic ischemia group demonstrated that the evoked potentials were suppressed. The P-P amplitudes at 0 h, 1 h, 2 h and 3 h were 13.98 ± 0.73%, 12.70 ± 0.85%, 14.06 ± 0.68% and 14.22 ± 1.57% of the baseline, respectively.

(C) The average SSEPs before and after stroke in the topiramate-treated photothrombotic ischemia group gradually recovered for up to 3 h after stroke. The P-P amplitudes at 0 h, 1 h, 2 h, and 3 h were 9.10 ± 1.47%, 28.98 ± 6.69%, 58.24 ± 5.38% and 77.25 ± 4.10% of the baseline, respectively.

(D) Comparison of P-P amplitudes among the control, photothrombotic ischemia and photothrombotic ischemia+topiramate groups. At 0 h–2 h after stroke, the evoked potentials in the photothrombotic ischemia group and the photothrombotic ischemia+topiramate group were significantly different from those in the control group ($p < 0.05$). At 3 h, the P-P amplitude in the photothrombotic ischemia group remained significantly lower than that in the control group ($p < 0.05$). There was no significant difference between the photothrombotic ischemia+topiramate group and the control group, demonstrating the recovery of neural function after topiramate treatment.

and suppress neuronal depolarization.[16] Our results provide critical *in vivo* evidence that PID velocity is not affected by topiramate treatment but rather significantly decreases the number of PIDs.

Typically, PID results in a decrease in the CBF, which in turn leads to an increase in infarct size. Compared with the middle cerebral artery occlusion method, intraluminal suturing of the middle cerebral artery damages the striatum and cortex, induces large-scale infarction, and produces large penumbra areas.[29,30] Therefore, the PID-induced CBF is significantly reduced. The PTI model we used creates a small infarct area, so tissue perfusion can be maintained through collateral circulation. Collateral circulation plays a crucial role in maintaining brain tissue perfusion during ischemic stroke, prolonging the time window for effective treatment and ultimately preventing the irreversible damage that may lead to worse clinical outcomes.

As shown in Figure 10, topiramate also reduced the infarct volume and preserved neurons, albeit in reduced numbers. This finding corroborates the study by Yang et al., in which the infarct volume was significantly reduced after topiramate treatment.[31] The ability of topiramate to reduce the influx of calcium ions can decrease their effects on proteases and lipases.[14] Inhibiting the activation of kinases, phosphatases, endonucleases, and free radicals prevents the decomposition of phospholipids, proteins, and nucleic acids. Ultimately, this could prevent the apoptosis cascade, improve the survival rate of peripheral neuronal cells, and reduce the scope of cerebral infarction.[11]

To further examine the effects of topiramate on neuronal cell death, inflammation, and neuronal repair after ischemic injury, we used Western blotting to measure the levels of proteins related to neuroprotection, including NeuN, ED1 (CD68), Iba-1, GFAP, BDNF, Bcl-2, and Bax, among which NeuN is a neuronal marker; ED1 (CD68) and Iba-1 are markers of inflammation, identifying macrophages and activated microglia, respectively[12]; GFAP is a marker of activated astrocytes[32]; and BDNF is associated with neuronal repair following injury.[3] In the ischemic core region, NeuN expression decreased after ischemia compared with that in the control group, while NeuN expression increased significantly after topiramate administration compared with that in the photothrombotic ischemia group (Figure 11B). Such a decrease in NeuN levels after photothrombotic ischemia is expected, as a large amount of calcium ions enter cells and promote the activation of enzymes and the generation of free radicals.[11,33] The influx of many calcium ions also causes mitochondria-mediated apoptosis and leads to neuronal death.[33] The administered topiramate binds to voltage-gated calcium channels, thereby preventing calcium ions from entering cells and reducing mitochondria-mediated apoptosis/neuronal death.

The Bcl-2 family of proteins, including Bcl-2 and Bax, regulate programmed cell death. Experimental studies have shown that overexpression of the antiapoptotic protein Bcl-2 can alleviate ischemic brain damage in animal models of stroke. Although activated Bax promotes cell death, these two molecules can move independently to modulate cell death. We observed Bcl-2 downregulation and Bax upregulation in photothrombotic ischemia. Moreover, the antiapoptotic protein Bcl-2 was upregulated and the proapoptotic protein Bax was downregulated in rats treated with topiramate. These observations clearly indicate that topiramate has a significant protective effect against photothrombotic ischemic injury, which may be due to its antiapoptotic potential.[34]

As shown in Figures 11C and 11D, ED1 (CD68) and Iba-1 expression increased significantly following ischemic stroke, while both decreased significantly in the ischemic core and peri-infarct areas following topiramate administration. These results confirmed the anti-inflammatory effects of topiramate. Similarly, GFAP expression increased after ischemic stroke but decreased significantly in the ischemic core, penumbra, and distant cortex after topiramate administration. We also found that BDNF expression increased in the ischemic core region after ischemic stroke but decreased after topiramate administration. In the penumbra region, neither NeuN nor BDNF expression decreased significantly

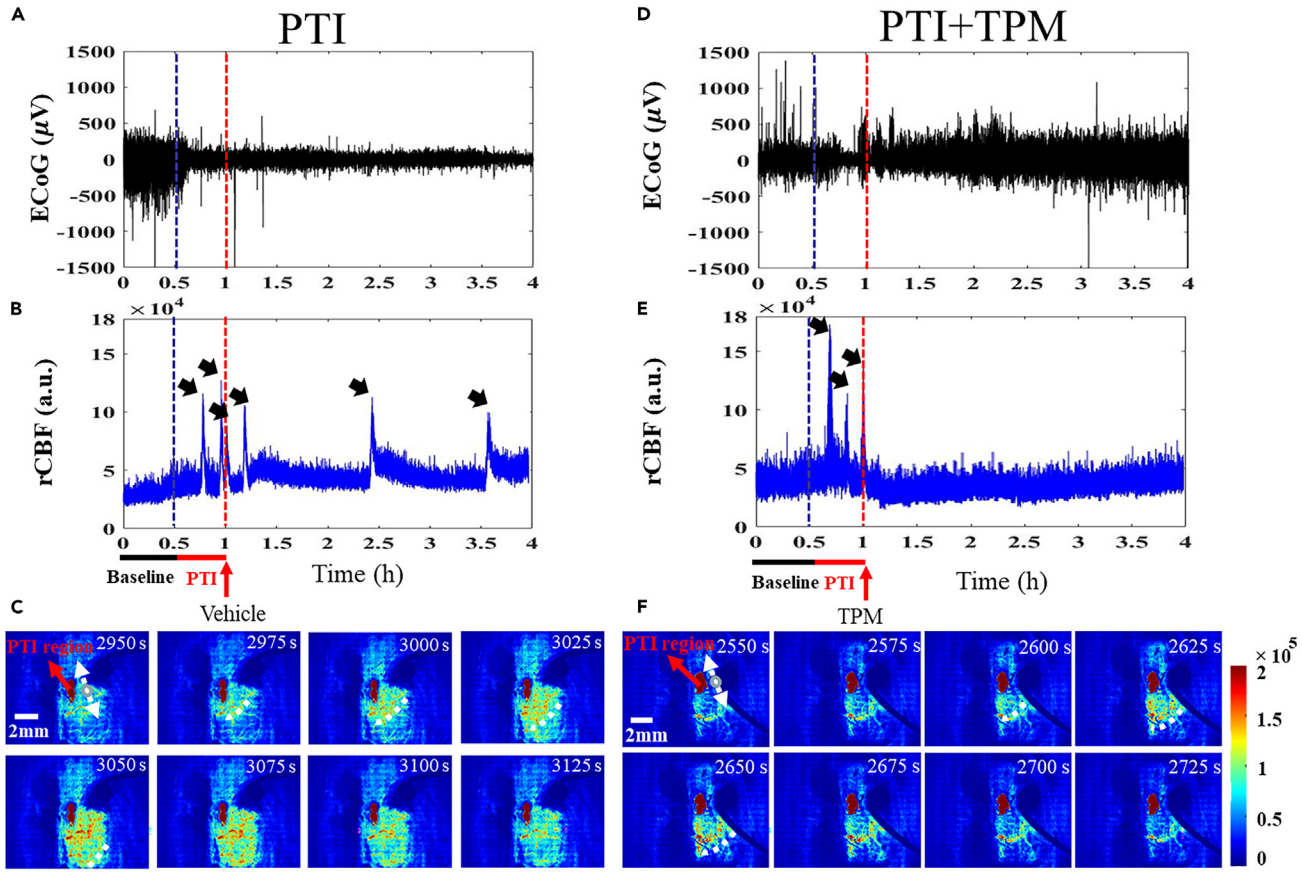

Figure 8. ECoG-LSCI was used to observe neurovascular function during photothrombotic ischemia-induced peri-infarct depolarization (PID)

(A) Electrophysiological changes in the ECoG signal after photothrombotic ischemia in rats without topiramate treatment. The electrophysiological signals were inhibited after stroke induction.

(B) The corresponding changes in CBF. Continuous PID progression could be observed after photothrombotic ischemia. Individual PID events are labeled with black arrows.

(C) Representative LSCI contrast images of PIDs after photothrombotic ischemia (Video S2). The white arrows represent the directions of PID propagation. The red arrow represents the PTI region.

(D) Electrophysiological changes in the ECoG signal after photothrombotic ischemia in rats treated with topiramate. The electrophysiological signals were inhibited after stroke induction, with gradual recovery after topiramate treatment.

(E) The corresponding changes in CBF. There were fewer PID events after topiramate administration.

(F) Representative LSCI contrast images of PID after photothrombotic ischemia and topiramate treatment (Video S2).

after photothrombotic ischemia, which is likely due to reduced neuronal damage that occurred outside the ischemic core. However, ED1 (CD68), Iba-1, and GFAP levels were significantly increased in the penumbra region after photothrombotic ischemia, suggesting that the inflammatory effect extends outside the ischemic core. Importantly, topiramate treatment significantly reduced the expression of ED1 (CD68), Iba-1 and GFAP in the penumbra region.

In the distant cortex region, no significant differences in NeuN, ED1 (CD68), Iba-1, or BDNF expression were detected between the different treatment groups. However, GFAP expression was significantly elevated in the distant cortex after photothrombotic ischemia, indicating that the surrounding normal astrocytes are affected, as discussed previously.[35]

Possible neuroprotective pathways of topiramate following photothrombotic ischemia

The process of brain injury during ischemic stroke and the possible protective mechanism of topiramate in stroke treatment are shown in Figure 12. Thrombus formation prevents blood from transporting nutrients such as oxygen and glucose.[36] A lack of oxygen and glucose prevents neurons from receiving sufficient ATP from glycolysis,[2,10] inhibiting the functions of sodium-potassium pumps and triggering ionic imbalance and depolarization, as shown in the primary damage pathway.[3] The release of large amounts of glutamate induces nerve excitotoxicity and promotes the entry of sodium and calcium ions into cells, leading to further cell depolarization and causing PID.[12] The entry of large amounts

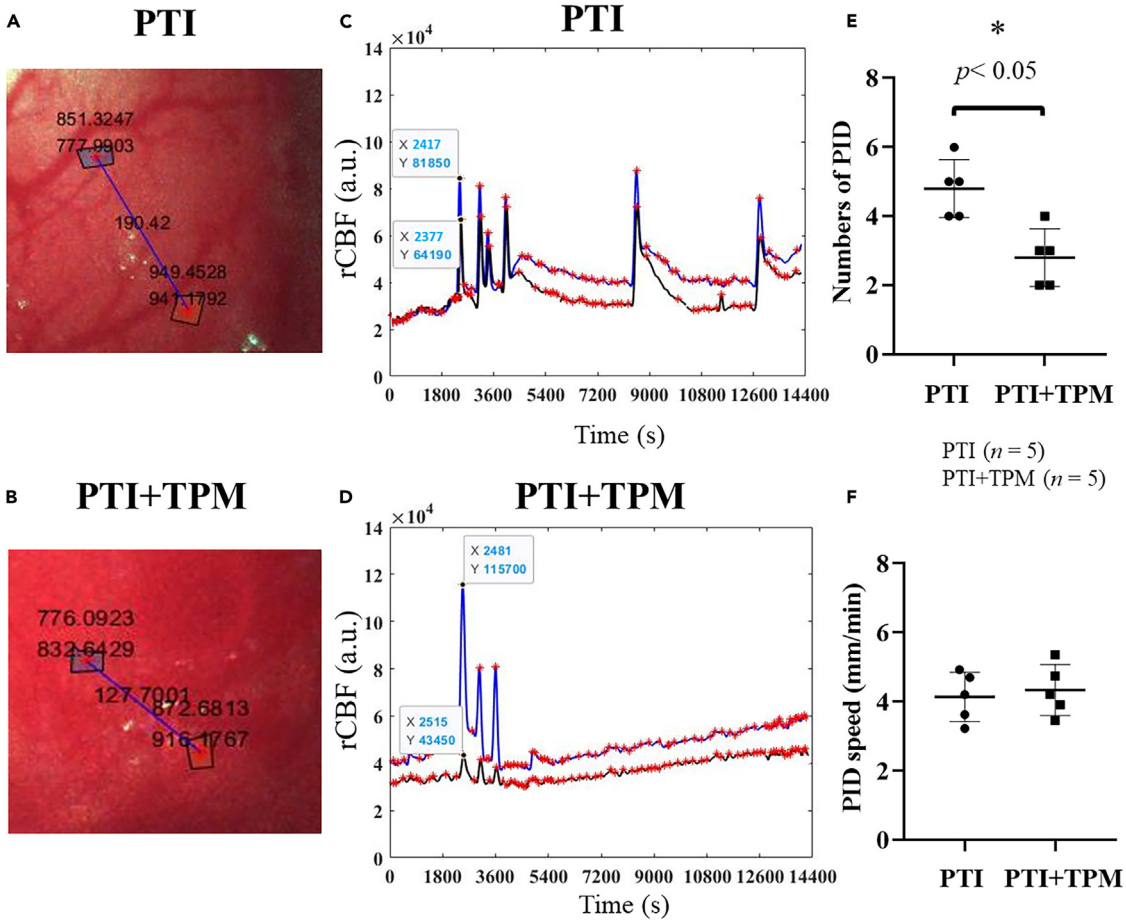

Figure 9. After topiramate treatment, the number of PIDs in the rats decreased significantly

(A and B) Representative CCD images of the cortical surface in the photothrombotic ischemia group and photothrombotic ischemia+topiramate administration group, respectively. The circled ROIs were used to calculate the PID speed.

(C and D) Representative plots of the CBF in the circled ROIs for the photothrombotic ischemia group and photothrombotic ischemia+topiramate administration group, respectively.

(E) After topiramate treatment, there were significantly fewer PIDs than that in the photothrombotic ischemia group ($p < 0.05$), showing that topiramate may offer neuroprotection. In the photothrombotic ischemia group, the average number of PIDs was 4.8 ± 0.4, while in the topiramate administration group, the average number of PIDs was 2.8 ± 0.4.

(F) Comparison of PID speed, showing no significant difference between the topiramate treatment group and the photothrombotic ischemia group. In the photothrombotic ischemia stroke group, the average PID speed was 4.14 ± 0.32 mm/min, while in the topiramate administration group, the average PID speed was 4.34 ± 0.33 mm/min. Data are represented as mean ± SD.

of calcium ions will activate lipases, proteases, phosphatases, kinases, free radicals, and endonucleases, which promote the decomposition of nucleic acids, proteins, and phospholipids and generate excess free radicals to induce cellular damage.[11]

In the secondary damage pathway, the large influx of calcium ions after photothrombotic ischemia also leads to the mitochondrial release of cytochrome *c*, triggering the sequential activation of caspase-9 and the effector caspase-3, resulting in apoptosis.[33] Such neuronal cell death after photothrombotic ischemia is associated with decreased expression of NeuN, as shown in Figure 11B.[36] The generation of free radicals induces an inflammatory response and the activation of microglia, as evidenced by the increase in ED1 (CD68) and Iba-1 expression (Figures 11C and 11D).[37] GFAP expression also increases in astrocytes in response to inflammation, as shown in Figure 11E. M1 microglia are then transformed into M2 cells that restore neuronal function, as shown by the increase in BDNF expression (Figure 11F).[38]

Topiramate has been shown to inhibit AMPAR and Ca^{2+} channel-related receptors, reducing the influx of sodium and calcium ions.[11,14] This mitigates the inflammatory response, inhibits calcium-induced apoptosis, and reduces the occurrence of PID.[14–16] Microglial activation, BDNF expression, and GFAP expression subsequently decrease, while NeuN expression levels remain similar to baseline, resulting in neuroprotection by topiramate.

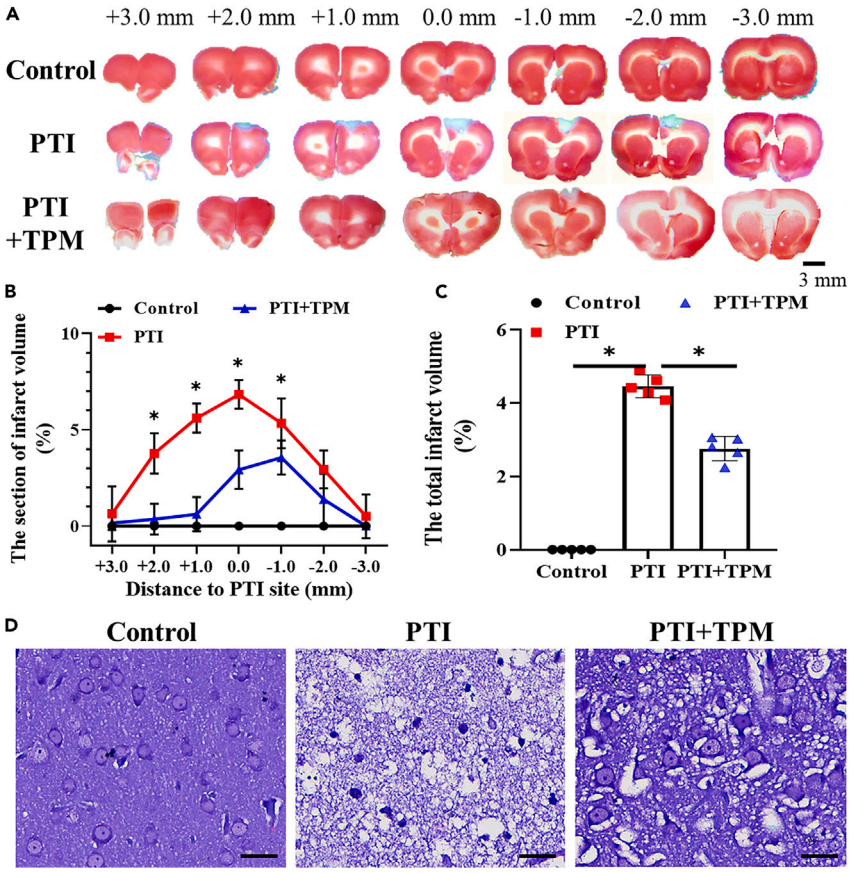

Figure 10. Analysis and quantification of infarct volume by TTC staining and Nissl staining

(A) Representative TTC staining images of coronal brain slices from the control (first row), photothrombotic ischemia (2nd row), and topiramate treatment groups (3rd row). The ischemia site was taken as 0 mm, and the brain was sliced in 1 mm increments up to ±3 mm. The stroke infarct area appears white and is indicated by the black arrow. The infarct volume was smaller in the topiramate treatment group than in the PTI only group.

(B) Quantified infarct volume after photothrombotic ischemia at different distances from the infarct site.

(C) Quantification of the total infarct volume as a percentage of the total brain tissue volume. In the stroke group, the average infarct volume was 4.5 ± 0.1%, while that in the photothrombotic ischemia+topiramate group was 2.8 ± 0.2%, indicating a significantly reduced infarct volume ($p < 0.05$).

(D) Nissl-stained brain tissue sections showing cerebral lesions caused by photochemical thrombosis in the rat brain. Scale bar: 40 μM. Data are represented as mean ± SD.

Conclusion

In this study, we developed an ECoG-LSCI system that combines laser speckle contrast imaging (LSCI) with electrocorticography (ECoG) to observe CBF and electrophysiology in real-time. We tested the feasibility of using our system in a photothrombotic ischemia model and observed changes in the hemodynamics and somatosensory evoked potentials (SSEPs) in the S1FL region induced by electrical stimulation. We found that topiramate, an antiepileptic drug, exerts neuroprotective effects on the brain. We administered topiramate to rats after the induction of photothrombotic ischemia and observed postischemic depolarizations (PIDs) to verify our hypothesis that topiramate could be used to treat PID. We found that topiramate effectively inhibited and reduced the PID frequency ($p < 0.05$) without affecting PID velocity. We also found that compared with photothrombotic ischemia, topiramate significantly reduced the infarct volume ($p < 0.05$). Our study suggested that topiramate has the potential to be considered an adjuvant therapy for stroke. Furthermore, we measured the expression levels of different markers in the ischemic core region after stroke and topiramate administration. We found increased expression of the inflammatory factors ED1 (CD68) and Iba-1 as well as GFAP, which promotes reactive gliosis and the formation of glial scars. The upregulation of these inflammatory factors indicates that neuronal cells are damaged, resulting in a decrease in NeuN expression. However, topiramate treatment significantly decreased the expression of ED1 (CD68), Iba-1, and GFAP, indicating a reduction in the inflammatory response. We also observed a significant decrease in the expression of BDNF, a protein involved in neuronal regeneration. In addition, our study demonstrated the feasibility and effectiveness of using the ECoG-LSCI system for studying cerebral neurovascular dynamics. Our findings provide valuable insights into translational stroke research and therapies.

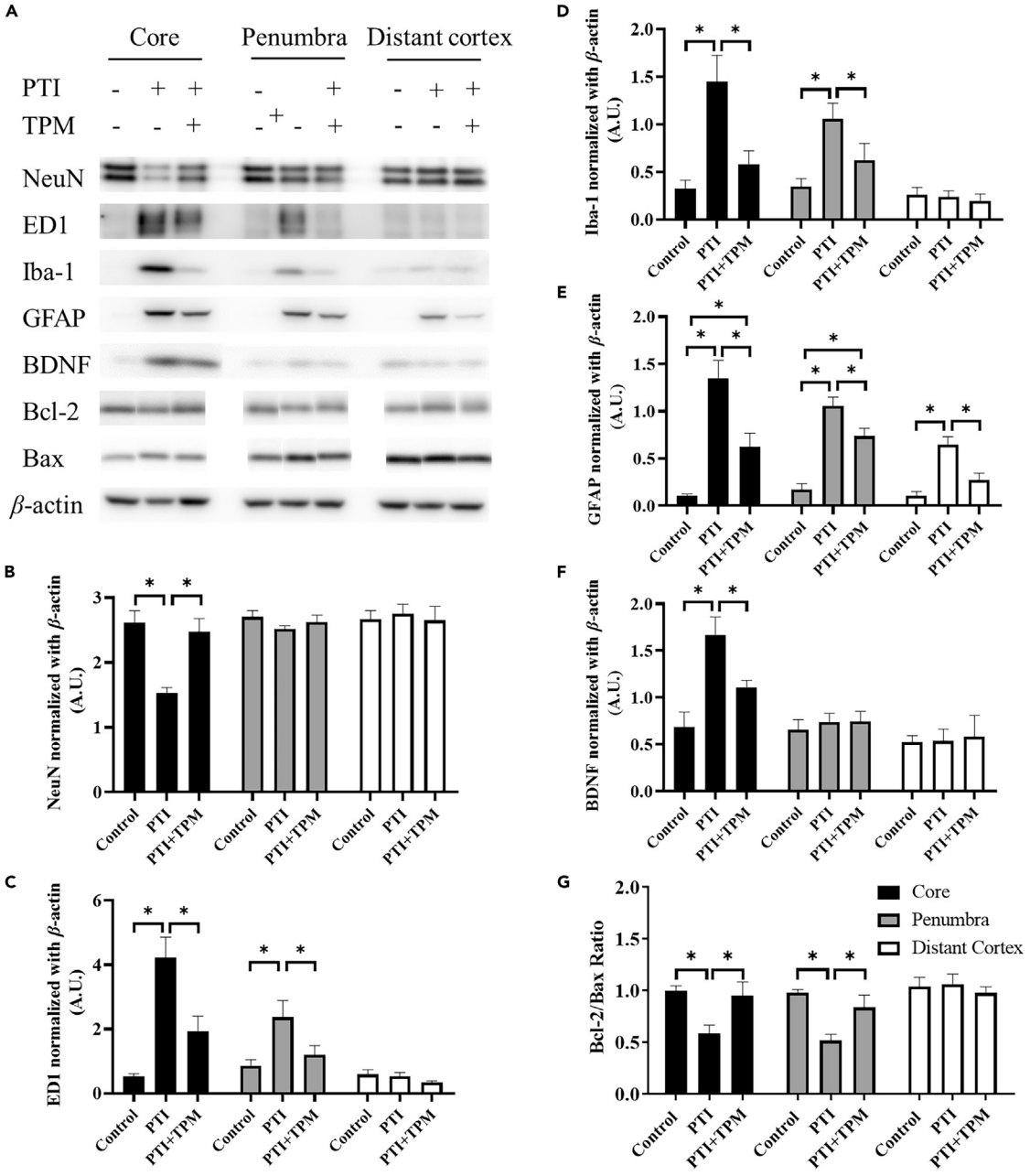

Figure 11. Western blotting showed that topiramate has the potential to reduce the side effects of stroke

(A) Western blots comparing the expression levels of NeuN, ED1 (CD68), Iba-1, GFAP, BDNF, Bcl-2, and Bax in the core, penumbra and distant cortex after photothrombotic ischemia.

(B) In the ischemic core region, NeuN expression was significantly lower in the photothrombotic ischemia group than in the control group ($p < 0.05$) and the topiramate treatment group ($p < 0.05$), demonstrating that topiramate has the potential to slow neuronal death.

(C) ED1 (CD68) expression in both the ischemic core and penumbra regions was significantly greater in the photothrombotic ischemia group than in the control ($p < 0.05$) and topiramate treatment groups ($p < 0.05$). This finding demonstrated that topiramate suppressed inflammation.

(D) Iba-1 expression in both the ischemic core and penumbra regions was significantly greater in the photothrombotic ischemia group than in the control ($p < 0.05$) and topiramate treatment groups ($p < 0.05$). This finding demonstrated that topiramate plays a role in suppressing Iba-1 expression.

(E) In all regions, GFAP expression was significantly greater in the photothrombotic ischemia group than in the control ($p < 0.05$) and topiramate treatment groups ($p < 0.05$). In the ischemic core and penumbra regions, GFAP expression was also significantly greater in the topiramate treatment group than in the control group ($p < 0.05$).

Figure 11. *Continued*

(F) BDNF expression in the ischemic core region was significantly greater in the photothrombotic ischemia group than in the control ($p < 0.05$) and topiramate treatment groups ($p < 0.05$).

(G) In the ischemic core and penumbra regions, Bcl-2/Bax expression was significantly lower in the photothrombotic ischemia group than in the control and topiramate treatment groups ($p < 0.05$). Data are represented as mean ± SD.

Limitations of the study

The photothrombotic stroke model utilizes local intravascular photooxidation to generate highly restricted ischemic cortical lesions. The advantages of this model are the small size of the infarct, the ability to place the infarct within different functional subregions of the cortex, and minimal surgical manipulation of the animal. The aim of this technology is to simulate human stroke by causing platelet aggregation, similar to cerebral ischemia. However, the photothrombotic damage caused by this technique is somewhat different from the damage caused by stroke in humans. First, thrombosis in the model is initiated in many blood vessels in the illuminated area, whereas stroke usually occurs due to the interruption of blood flow in a single terminal artery. Therefore, certain brain regions that are only partially supported by the affected arteries are initially less affected after stroke because they may receive blood from collateral arteries and do not undergo necrotic cell death. In contrast, the well-defined borders produced by photothrombosis result in a very limited penumbra, which is the primary target of postischemic neuroprotective agents. Furthermore, in some stroke patients, reperfusion occurs spontaneously, which may lead to secondary insults, including reperfusion injury. To study this specific aspect of ischemia, a transient occlusion model is more appropriate.

The infarct pattern in photothrombotic lesions exhibits some characteristics that differ from those of human stroke. MRI images reveal that in photothrombotic lesions, ischemic infarction and angioedema occur simultaneously, while in human stroke, ischemic infarction is more common than angioedema. However, a photothrombosis model may not be sufficient to study antithrombotic drugs because

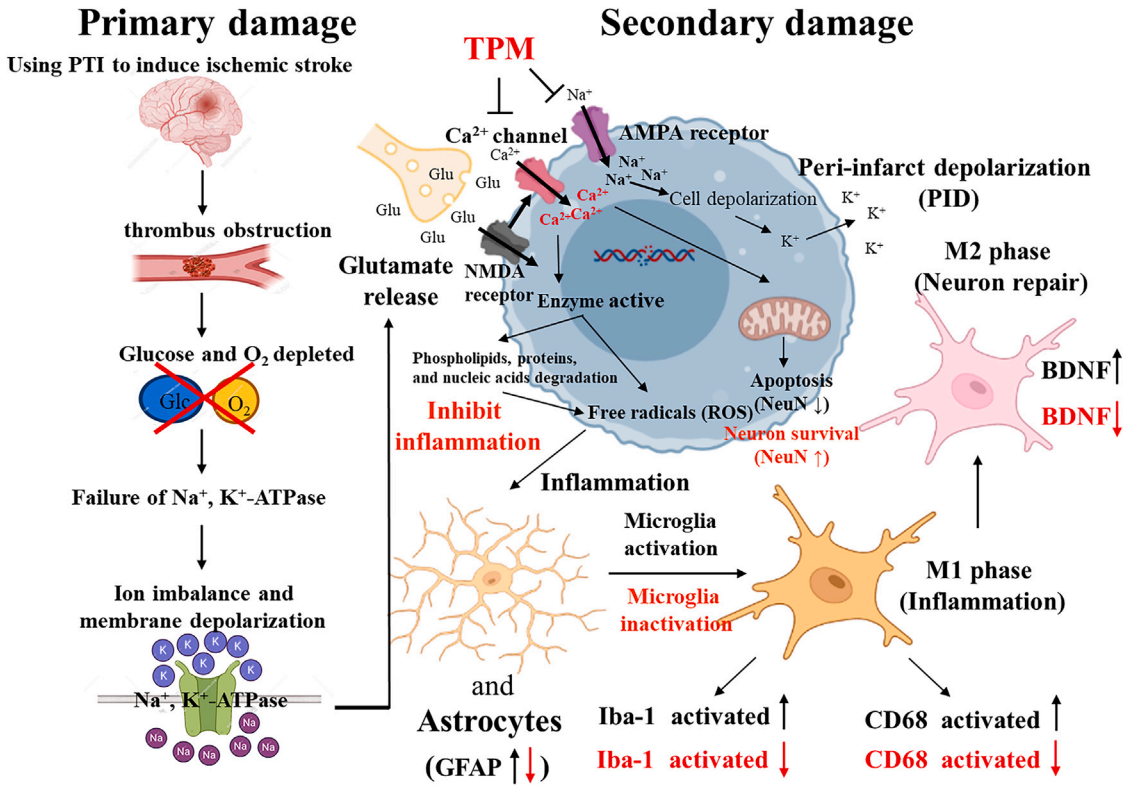

Figure 12. Flow diagram of brain injury after ischemic stroke and the neuroprotective effect of topiramate

Ischemic stroke is induced during thrombus formation. This prevents neurons from obtaining sufficient ATP from glycolysis, inhibiting the function of the sodium-potassium pump and triggering ionic imbalance and depolarization. Additionally, large amounts of glutamate are released, which induces nerve excitotoxicity and promotes the entry of sodium and calcium ions into cells. Cellular depolarization occurs along with potassium ion release and PID. The entry of a large amount of calcium ions activates a cascade of inflammation and apoptosis. The inflammatory response and the activation of microglia to an acute M1 inflammatory state increase the expression of Iba-1 and ED1 (CD68), which are associated with phagocytosis. GFAP expression also increases in astrocytes. M1 microglia are transformed into the M2 phenotype for neuronal repair, and BDNF expression increases. The activation of apoptosis results in decreased NeuN expression. The neuroprotective effects of topiramate treatment are indicated in red. The inhibition of AMPAR and Ca^{2+} channel-related receptors by topiramate reduces the influx of sodium and calcium ions, preventing downstream reactions, including PID, inflammation and apoptosis. The expression levels of Iba-1, ED1 (CD68) and GFAP decrease. Due to reduced apoptosis, the decrease in NeuN expression is alleviated.

photothrombotic infarction can occur even after platelet blockade or inhibition of the intrinsic coagulation pathway. Some studies suggest that in certain cases, platelet coagulation may not be necessary for photothrombotic occlusion, which may occur due to disruption of the endothelial integrity and lead to edema and peripheral vascular compression.[39]

STAR★METHODS

Detailed methods are provided in the online version of this paper and include the following:

- KEY RESOURCES TABLE
- RESOURCE AVAILABILITY
  - Lead contact
  - Materials availability
  - Data and code availability
- EXPERIMENTAL MODEL AND STUDY PARTICIPANT DETAILS
  - Photothrombotic technique for focal ischemic stroke induction
- METHOD DETAILS
  - The ECoG-LSCI system
  - Animal preparation and craniotomy
  - KCl-induced CSD
  - Peripheral electrical stimulation
  - LSCI data analysis
  - Data analysis of the ECoG recordings
  - Quantification of the infarct volume
  - Nissl staining
  - Western blotting
- QUANTIFICATION AND STATISTICAL ANALYSIS

SUPPLEMENTAL INFORMATION

Supplemental information can be found online at https://doi.org/10.1016/j.isci.2024.110033.

ACKNOWLEDGMENTS

This research was supported in part by the National Science and Technology Council of Taiwan under grant numbers 110-2221-E-400-003-MY3, 111-3114-8-400-001, 111-2314-B-075-006, 111-2221-E-035-015, 111-2218-E-007-019, 112-2629-E-400-001; and by the National Health Research Institutes of Taiwan under grant numbers NHRI-EX111-11111EI, and NHRI-EX111-11129EI and by the Ministry of Health and Welfare, Taiwan under grant numbers MOHW 112-0324-01-30-06 and MOHW 113-0324-01-30-11, and by the Metal Industries Research & Development Centre under grant number 112-EC-17-A-22-1851.

AUTHOR CONTRIBUTIONS

Y.W. and Y.L.C. carried out the *in vitro* and *in vivo* experiments. Y.W., Y.Y.I.S., S.Y., Y.L.C., L.T.C., and L.D.L. drafted the manuscript. Y.W., Y.Y.I.S., L.T.C., and L.D.L. conceived and supervised the study. S.Y. and L.D.L. revised the manuscript. Y.Y.I.S., L.T.C., and L.D.L. discussed the experimental design and revised the manuscript. All authors discussed the data and commented on the manuscript.

DECLARATION OF INTERESTS

The authors declare no conflicts of interest.

Received: December 5, 2023
Revised: April 18, 2024
Accepted: May 16, 2024
Published: May 23, 2024

REFERENCES

1. Orellana-Urzúa, S., Rojas, I., Líbano, L., and Rodrigo, R. (2020). Pathophysiology of ischemic stroke: role of oxidative stress. Curr. Pharm. Des. *26*, 4246–4260.
2. Prabhakaran, S., Ruff, I., and Bernstein, R.A. (2015). Acute stroke intervention: a systematic review. JAMA *313*, 1451–1462.
3. Liu, W., Wang, X., O'Connor, M., Wang, G., and Han, F. (2020). Brain-derived neurotrophic factor and its potential therapeutic role in stroke comorbidities. Neural Plast. *2020*, 1969482.
4. Kao, Y.-C.J., Li, W., Lai, H.-Y., Oyarzabal, E.A., Lin, W., and Shih, Y.-Y.I. (2014). Dynamic perfusion and diffusion MRI of cortical spreading depolarization in photothrombotic ischemia. Neurobiol. Dis. *71*, 131–139.
5. Smith, J.M., Bradley, D.P., James, M.F., and Huang, C.L.-H. (2006). Physiological studies

of cortical spreading depression. Biol. Rev. *81*, 457–481.
6. Shih, Y.-Y.I., Yash, T.V., Rogers, B., and Duong, T.Q. (2014). FMRI of deep brain stimulation at the rat ventral posteromedial thalamus. Brain Stimul. *7*, 190–193.
7. Dreier, J.P., Fabricius, M., Ayata, C., Sakowitz, O.W., Shuttleworth, C.W., Dohmen, C., Graf, R., Vajkoczy, P., Helbok, R., Suzuki, M., et al. (2017). Recording, analysis, and interpretation of spreading depolarizations in neurointensive care: review and recommendations of the COSBID research group. J. Cereb. Blood Flow Metab. *37*, 1595–1625.
8. Dreier, J.P. (2011). The role of spreading depression, spreading depolarization and spreading ischemia in neurological disease. Nat. Med. *17*, 439–447.
9. Strong, A.J., Anderson, P.J., Watts, H.R., Virley, D.J., Lloyd, A., Irving, E.A., Nagafuji, T., Ninomiya, M., Nakamura, H., Dunn, A.K., and Graf, R. (2007). Peri-infarct depolarizations lead to loss of perfusion in ischaemic gyrencephalic cerebral cortex. Brain *130*, 995–1008.
10. Barthels, D., and Das, H. (2020). Current advances in ischemic stroke research and therapies. Biochim. Biophys. Acta, Mol. Basis Dis. *1866*, 165260.
11. Weber, J.T. (2012). Altered calcium signaling following traumatic brain injury. Front. Pharmacol. *3*, 25302.
12. Barone, F.C., and Feuerstein, G.Z. (1999). Inflammatory mediators and stroke: new opportunities for novel therapeutics. J. Cereb. Blood Flow Metab. *19*, 819–834.
13. Kramer, D.R., Fujii, T., Ohiorhenuan, I., and Liu, C.Y. (2016). Cortical spreading depolarization: Pathophysiology, implications, and future directions. J. Clin. Neurosci. *24*, 22–27.
14. Spritzer, S.D., Bravo, T.P., and Drazkowski, J.F. (2016). Topiramate for treatment in patients with migraine and epilepsy. Headache J. Head Face Pain *56*, 1081–1085.
15. Colombo, B., Dalla Libera, D., Annovazzi, P.O., and Comi, G. (2008). Headache therapy with neuronal stabilising drugs. Neurol. Sci. *29*, 131–136.
16. DeLorenzo, R.J., Sombati, S., and Coulter, D.A. (2000). Effects of topiramate on sustained repetitive firing and spontaneous recurrent seizure discharges in cultured hippocampal neurons. Epilepsia *41*, 40–44.
17. Sanchez-del-Rio, M., Reuter, U., and Moskowitz, M.A. (2006). New insights into migraine pathophysiology. Curr. Opin. Neurol. *19*, 294–298.
18. Sarangi, P., and Pal, P. (2019). Superresolution via bilinear fusion of multimodal imaging data. SPIE *10989*, 128–134.
19. Ma, Y., Yang, D., Bai, J., Zhao, Y., Hu, Q., and Yu, C. (2022). Time trends in stroke and subtypes mortality attributable to household air pollution in Chinese and Indian adults: an age-period-cohort analysis using the global burden of disease study 2019. Front. Aging Neurosci. *14*, 740549.
20. Liao, L.-D., Bandla, A., Ling, J.M., Liu, Y.-H., Kuo, L.-W., Chen, Y.-Y., King, N.K., Lai, H.-Y., Lin, Y.-R., and Thakor, N.V. (2014). Improving neurovascular outcomes with bilateral forepaw stimulation in a rat photothrombotic ischemic stroke model. Neurophotonics *1*, 011007.
21. Mohajerani, M.H., Aminoltejari, K., and Murphy, T.H. (2011). Targeted mini-strokes produce changes in interhemispheric sensory signal processing that are indicative of disinhibition within minutes. Proc. Natl. Acad. Sci. USA *108*, E183–E191.
22. Armitage, G.A., Todd, K.G., Shuaib, A., and Winship, I.R. (2010). Laser speckle contrast imaging of collateral blood flow during acute ischemic stroke. J. Cereb. Blood Flow Metab. *30*, 1432–1436.
23. Donmez-Demir, B., Erdener, Ş.E., Karatas, H., Kaya, Z., Ulusoy, I., and Dalkara, T. (2020). KCl-induced cortical spreading depression waves more heterogeneously propagate than optogenetically-induced waves in lissencephalic brain: An analysis with optical flow tools. Sci. Rep. *10*, 12793.
24. Kaufmann, D., Theriot, J.J., Zyuzin, J., Service, C.A., Chang, J.C., Tang, Y.T., Bogdanov, V.B., Multon, S., Schoenen, J., Ju, Y.S., and Brennan, K.C. (2017). Heterogeneous incidence and propagation of spreading depolarizations. J. Cereb. Blood Flow Metab. *37*, 1748–1762.
25. Eiselt, M., Gießler, F., Platzek, D., Haueisen, J., Zwiener, U., and Röther, J. (2004). Inhomogeneous propagation of cortical spreading depression—detection by electro- and magnetoencephalography in rats. Brain Res. *1028*, 83–91.
26. Sanders, L., Tan, M., Cook, M., and D'Souza, W. (2015). Stroke Prevalence and Incidence of Post-stroke Seizures: Analysis of the Tasmanian Epilepsy Register (WILEY-BLACKWELL 111 RIVER ST, HOBOKEN 07030-5774), p. 47.
27. White, H.S., Brown, S.D., Woodhead, J.H., Skeen, G.A., and Wolf, H.H. (1997). Topiramate enhances GABA-mediated chloride flux and GABA-evoked chloride currents in murine brain neurons and increases seizure threshold. Epilepsy Res. *28*, 167–179.
28. McLean, M.J., Bukhari, A.A., and Wamil, A.W. (2000). Effects of topiramate on sodium-dependent action-potential firing by mouse spinal cord neurons in cell culture. Epilepsia *41*, 21–24.
29. Unekawa, M., Tomita, Y., Masamoto, K., Kanno, I., Nakahara, J., and Izawa, Y. (2022). Close association between spreading depolarization and development of infarction under experimental ischemia in anesthetized male mice. Brain Res. *1792*, 148023.
30. Lunardi Baccetto, S., and Lehmann, C. (2019). Microcirculatory changes in experimental models of stroke and CNS-injury induced immunodepression. Int. J. Mol. Sci. *20*, 5184.
31. Yang, Y., Li, Q., Miyashita, H., Howlett, W., Siddiqui, M., and Shuaib, A. (2000). Usefulness of postischemic thrombolysis with or without neuroprotection in a focal embolic model of cerebral ischemia. J. Neurosurg. *92*, 841–847.
32. Amalia, L. (2021). Glial fibrillary acidic protein (GFAP): Neuroinflammation biomarker in acute ischemic stroke. J. Inflamm. Res. *14*, 7501–7506.
33. Kondratskyi, A., Kondratska, K., Skryma, R., and Prevarskaya, N. (2015). Ion channels in the regulation of apoptosis. Biochim. Biophys. Acta *1848*, 2532–2546.
34. Yaidikar, L., and Thakur, S. (2015). Punicalagin attenuated cerebral ischemia–reperfusion insult via inhibition of proinflammatory cytokines, up-regulation of Bcl-2, down-regulation of Bax, and caspase-3. Mol. Cell. Biochem. *402*, 141–148.
35. Huang, L., Wu, Z.-B., ZhuGe, Q., Zheng, W., Shao, B., Wang, B., Sun, F., and Jin, K. (2014). Glial scar formation occurs in the human brain after ischemic stroke. Int. J. Med. Sci. *11*, 344–348.
36. Dunn, A.K. (2012). Laser speckle contrast imaging of cerebral blood flow. Ann. Biomed. Eng. *40*, 367–377.
37. Fu, R., Shen, Q., Xu, P., Luo, J.J., and Tang, Y. (2014). Phagocytosis of microglia in the central nervous system diseases. Mol. Neurobiol. *49*, 1422–1434.
38. Chen, A., Xiong, L.-J., Tong, Y., and Mao, M. (2013). The neuroprotective roles of BDNF in hypoxic ischemic brain injury. Biomed. Rep. *1*, 167–176.
39. Labat-Gest, V., and Tomasi, S. (2013). Photothrombotic ischemia: a minimally invasive and reproducible photochemical cortical lesion model for mouse stroke studies. JoVE *76*, e50370.
40. Cheng, H., Luo, Q., Zeng, S., Chen, S., Cen, J., and Gong, H. (2003). Modified laser speckle imaging method with improved spatial resolution. J. Biomed. Opt. *8*, 559–564.
41. Briers, J.D., and Fercher, A.F. (1982). Retinal blood-flow visualization by means of laser speckle photography. Invest. Ophthalmol. Vis. Sci. *22*, 255–259.
42. Sigal, I., Gad, R., Caravaca-Aguirre, A.M., Atchia, Y., Conkey, D.B., Piestun, R., and Levi, O. (2013). Laser speckle contrast imaging with extended depth of field for in-vivo tissue imaging. Biomed. Opt Express *5*, 123–135.
43. Pan, H.-C., Liao, L.-D., Lo, Y.-C., Chen, J.-W., Wang, H.-L., Yang, L., Liang, Y.-W., Huang, P.-Y., Yang, M.-H., and Chen, Y.-Y. (2017). Neurovascular function recovery after focal ischemic stroke by enhancing cerebral collateral circulation via peripheral stimulation-mediated interarterial anastomosis. Neurophotonics *4*, 035003.
44. Li, H., Liu, Q., Lu, H., Li, Y., Zhang, H.F., and Tong, S. (2014). Directly measuring absolute flow speed by frequency-domain laser speckle imaging. Opt Express *22*, 21079–21087.
45. Benedek, A., Móricz, K., Jurányi, Z., Gigler, G., Lévay, G., Hársing, L.G., Jr., Mátyus, P., Szénási, G., and Albert, M. (2006). Use of TTC staining for the evaluation of tissue injury in the early phases of reperfusion after focal cerebral ischemia in rats. Brain Res. *1116*, 159–165.
46. Isayama, K., Pitts, L.H., and Nishimura, M.C. (1991). Evaluation of 2, 3, 5-triphenyltetrazolium chloride staining to delineate rat brain infarcts. Stroke *22*, 1394–1398.
47. Huang, A., Chen, Y., Wang, S., Du, H., Guan, A., Wu, H., Zhai, Q., Duan, N., Li, X., Zhao, P., et al. (2023). Esketamine ameliorates post-stroke anxiety by modulating microglial HDAC3/NF-κB/COX1 inflammatory signaling in ischemic cortex. Eur. J. Pharmacol. *947*, 175667.
48. Ma, C., Wang, X., Xu, T., Zhang, S., Liu, S., Zhai, C., Wang, Z., Mu, J., Li, C., Cheng, F., and Wang, Q. (2020). An integrative pharmacology-based analysis of refined qingkailing injection against cerebral ischemic stroke: a novel combination of baicalin, geniposide, cholic acid, and hyodeoxycholic acid. Front. Pharmacol. *11*, 519.

49. Bandla, A., Liao, L.-D., Chan, S.J., Ling, J.M., Liu, Y.-H., Shih, Y.-Y.I., Pan, H.-C., Wong, P.T.-H., Lai, H.-Y., King, N.K.K., et al. (2018). Simultaneous functional photoacoustic microscopy and electrocorticography reveal the impact of rtPA on dynamic neurovascular functions after cerebral ischemia. J. Cereb. Blood Flow Metab. *38*, 980–995.

50. Liu, Y.-H., Liao, L.-D., Tan, S.S.H., Kwon, K.Y., Ling, J.M., Bandla, A., Shih, Y.-Y.I., Tan, E.T.W., Li, W., Ng, W.H., et al. (2015). Assessment of neurovascular dynamics during transient ischemic attack by the novel integration of micro-electrocorticography electrode array with functional photoacoustic microscopy. Neurobiol. Dis. *82*, 455–465.

STAR★METHODS

KEY RESOURCES TABLE

REAGENT or RESOURCE	SOURCE	IDENTIFIER
Antibodies		
rabbit anti-NeuN	Abcam	Cat#ab177487; RRID:AB_2532109
rabbit anti-BDNF	Abcam	Cat#ab108319; RRID:AB_10862052
rabbit anti-CD68 (ED1)	Abcam	Cat#ab125212; RRID:AB_10975465
goat anti-Iba-1	Abcam	Cat#ab5076; RRID:AB_2224402
goat anti-GFAP	Santa Cruz Biotechnology	Cat#sc-6170; RRID:AB_641021
rabbit anti-BAX	Proteintech	Cat#50599-2-Ig; RRID:AB_2061561
mouse anti-Bcl-2	Proteintech	Cat#68103-1-Ig; RRID:AB_2923635
mouse anti-β-actin	Santa Cruz Biotechnology	Cat#sc-47778; RRID:AB_626632
Chemicals, peptides, and recombinant proteins		
Rose Bengal	Sigma–Aldrich Corp	Cat# R3877
2,3,5-triphenyltetrazolium chloride	Sigma–Aldrich Corp	Cat#T8877
RIPA buffer	Visual Protein	Cat# RP05-100
Critical commercial assays		
BCA protein assay kit	ThermoFisher	Cat# 23225, 23227
Immobilon Western Chemiluminescent HRP Substrate	Millipore	WBKLS0500
Experimental models: Organisms/strains		
Rat: Sprague–Dawley	LASCO	N/A
Software and algorithms		
ImageJ	ImageJ	https://imagej.nih.gov/ij/index.html
GraphPad Prism v.8.0.1	GraphPad	https://www.graphpad.com/scientific-software/prism

RESOURCE AVAILABILITY

Lead contact

Further information and requests for resources and reagents should be directed to and will be fulfilled by the lead contact, Lun-De Liao (ldliao@nhri.edu.tw).

Materials availability

This study did not generate new unique reagents.

Data and code availability

- Original western blot images reported in this paper will be shared by the lead contact upon request.
- All original code will be shared by the lead contact upon request.
- Any addition information required to reanalyze the data reported in this paper is available from the lead contact Lun-De Liao (ldliao@nhri.edu.tw) upon request.

EXPERIMENTAL MODEL AND STUDY PARTICIPANT DETAILS

Photothrombotic technique for focal ischemic stroke induction

In this study, a blood vessel was targeted in the S1FL of the right hemisphere for focal photothrombotic ischemia.[20] An arteriole was chosen based on its appearance and location within a forelimb somatosensory diagram.[21] To induce photothrombotic ischemia, Rose Bengal, a photosensitizer (Na^+ salt, R3877; Sigma–Aldrich Corp., St. Louis, MO, USA), was first dissolved in saline to a concentration of 10 mg/mL. Anesthetized rats on a stereotaxic platform were then treated with 20 mg/kg body weight Rose Bengal solution through the tail vein. After injecting the Rose Bengal solution, a surface arteriole was targeted for occlusion with a 1-mm optic patch cable, which delivered a green light laser. The

fiber was connected to a laser power supply (532 nm, Shanghai Dream Lasers Technology Co., Ltd., Shanghai, China), and the surface of the target arteriole was illuminated for 30 min until an obstructive thrombus formed.[20]

METHOD DETAILS

The ECoG-LSCI system

The ECoG-LSCI platform, which integrates ECoG recording and an LSCI instrument to simultaneously measure neuronal activity and CBF, is shown in Figure 1. First, the relative cerebral blood flow (hereafter denoted CBF for all experimental data presented) was assessed using an LSCI system developed in the laboratory. The region of interest (ROI) was illuminated with a laser module (660/532 nm; 100 mW; RM-CW04-100, Unice E-O Service Inc., Taoyuan, Taiwan). A plano-convex lens (f = 75 mm, LA1608-A, Thorlabs Inc., Newton, NJ, USA) was used to expand the laser bundle to approximately 40 × 30 mm and supply appropriate lighting for the exposed area of the cerebral cortex. A 16-bit charge-coupled device (CCD) camera (pixel size: 4.65 × 4.65 μm, DR2-08S2M/C-EX-CS, Point Gray Research Inc., Richmond, BC, Canada) was used to image the illuminated region through a controllable amplification lens (0.3–1×, f/4.5 max) with a 2× expander. A linear polarizer was placed in front of the CCD image acquisition lens, and the working distance was set to approximately 5 cm to eliminate scattering. Laser speckle images (1032 × 776 pixels) were acquired at 2 fps (exposure time T = 10 ms).

The developed LSCI system was manipulated using a customized LabVIEW program (National Instruments, Austin, TX, USA). The changes in the CBF in the selected ROI were determined throughout the experiment. The changes in CBF in the cortex were then calculated and averaged. Therefore, laser speckle contrast analysis was performed using MATLAB (MATLAB R2020a, MathWorks Inc., Natick, MA, USA). Our LSCI data processing skeleton introduced a graphics processing unit (GPU) to enable real-time, high-resolution visualization of the bloodstream on a computer. NVIDIA (Santa Clara, CA, USA) designed the approach for the parallel computing platform (PCP) and programming model for the calculations. The high power of the GPU (GeForce GTX 650 Ti, NVIDIA, Santa Clara, CA, USA) significantly improved the computational performance.

A multichannel digital collection system (Blackrock Microsystems, Salt Lake City, Utah, USA) was used to measure somatosensory evoked potential (SSEP) signals on the PC. The ECoG signals were recorded via a preamplifier (gain of 2) and filtered through a bandpass filter from 0.5 Hz to 7,500 Hz. The filter was used to digitize the signals at a sampling rate of 10 kHz, and then, 150 Hz low-pass and 250 Hz high-pass filters were used to compare the electrophysiological changes in the peripherally stimulated cortex after photothrombotic ischemia.

Animal preparation and craniotomy

All procedures were guided by and received authorization from the Institutional Animal Care and Use Committee (IACUC) of the National Health Research Institute (NHRI, Taiwan) (IACUC number: NHRI-IACUC-107100-A). Thirteen male adult Sprague–Dawley (SD) rats ranging in weight from 250 to 350 g were divided into three groups to compare the neuroprotective effects of topiramate treatment after ischemic photothrombotic ischemia modeling by applying peripheral electrical stimulation; the groups included the control (n = 3), photothrombotic ischemia (n = 5) and photothrombotic ischemia+topiramate (n = 5) groups. The ECoG-LSCI system was used to measure changes in the CBF and ECoG in the ischemic brain area. The animals were housed on a 12-h dark/light cycle with consistent humidity and temperature and had free access to water and food.

Rats were anesthetized with 2–3% isoflurane (Bowlin Biotech Corp., Taipei, Taiwan) in oxygen. The depth of anesthesia was verified by examining the hindlimb withdrawal reflex of the rats before the surgical operation. A stereotaxic holder was used to fix the rats and reduce movement artifacts during cranial surgery after preparation for surgery (anesthesia and hair shaving). The skin and muscle were removed from the cranium to expose the bregma and the reference point, which was implanted on the lambda. Two experimental systems, including an LSCI instrument and an ECoG recording system, were used in the experiments to synchronously assess the changes in neurovascular parameters before/after photothrombotic ischemia, as shown in Figure 1. In the LSCI setup, the cranium was removed to create an 8 × 4.5 mm^2 window above the dura (while the dura remained intact) in the right hemisphere (anterior-posterior [AP] = ± 4 mm, medial-lateral [ML] = 0 to 4.5 mm). Furthermore, photothrombotic ischemia was induced in the vessels near the cortical area of the primary somatosensory forelimb (S1FL) (Figure 1). In the ECoG recording system, one of the epidural electrodes was placed at the S1FL (AP = + 1.0 mm, ML = + 4.0 mm), and a reference electrode was implanted at +3 mm ML from lambda on the right hemisphere and secured to the skull.

KCl-induced CSD

Here, we describe the KCl-induced CSD experimental protocol and our method for calculating CSD speed. Pictures of the rat brain under the CCD are shown in Figure 2A. The two-point mark (AP = + 1.0 mm, ML = 0.0 mm; AP = - 2.0 mm, ML = 0.0 mm) on the left half of the figure is the scale used to calculate CSD speed. The distance between the two points was 3 mm, and the electrode (screw) on the upper right was mainly used to receive the ECoG signals from the rats. A hole (AP = - 5.0 mm, ML = + 4.0 mm) was drilled at the bottom right above the dura to add KCl (potassium chloride, crystal, Avantor Inc., Radnor, Pennsylvania, USA) to induce CSD. The protocol for KCl-induced CSD is shown in Figure 2B. Before adding KCl, the LSCI and ECoG signals were recorded for 10 min as the baseline, and then CSD was induced with 1 M and 4 M KCl (dissolved in ddH_2O) for 60 min and recorded by the ECoG-LSCI system. Figure 2C shows the number of CSDs and the time of CSD occurrence. MATLAB was used to analyze all images and encircle two specific ROIs in the image (Figure 2D). Since CSDs were initiated from the hole through which KCl was administered, MATLAB was used to analyze the time difference between the two ROIs. Then, the scale in the image was used to calculate the actual distance between the two ROIs, thereby giving the CSD speed in mm/min using Equation 1. Figure 2E

shows the time point at which the CSD reached the two target ROIs to determine the time difference between the two ROIs. The black line is the time from the CSD wave to ROI region 1 (t1), and the blue line is the time from the CSD wave to ROI region 2 (t2). The difference between the 2 time points was calculated to obtain the time difference of the CSD reaching the 2 ROIs (Δt = t2 - t1). Therefore, the CSD speed formula was calculated as *X* (*Distance*) mm/Δt min, using Equation 2.

$$X\ (Distance)\ =\ (P1P2 \rightharpoonup) * X\ mm) / (R1R2 \rightharpoonup) * 3\ mm) \quad \text{(Equation 1)}$$

$$CSD\ speed\ =\ \frac{X\ (Distance)}{\Delta t\ (t2\ -\ t1)} \quad \text{(Equation 2)}$$

Peripheral electrical stimulation

The cranial window contained the epidural electrode in the S1FL area (AP: +1 mm, ML: +4 mm) and the reference electrode approximately 3 mm to the right of lambda to receive the ECoG signal, as shown in Figure 3A (scale bar, 2 mm). The purpose of this experiment was to assess the effects of topiramate on the CBF and electrophysiology of the neurovascular system in the rats in group 1 to group 3 after photothrombotic ischemia. Before photothrombotic ischemia was induced, the baseline electrical stimulation, LSCI, and ECoG signals were recorded, and electrical stimulation was recorded at 1-h intervals after the induction of photothrombotic ischemia, followed by TTC staining 24 h after photothrombotic ischemia initiation. The aim of the group 4 and group 5 experiments was to observe the progression of photothrombotic ischemia-induced PID and the effect of topiramate treatment. Before photothrombotic ischemia was induced, the LSCI and ECoG signals were recorded at baseline and then consecutively for up to 3 h after photothrombotic ischemia stroke, followed by TTC staining at 24 h after photothrombotic ischemia induction, as shown in Figure 3B.

The positive needle electrode was inserted into the contralateral forepaw from the palm to the arm, and the negative electrode needle was inserted into the arm. The forelimb was stimulated by applying rectangular pulses with a duration of 0.2 ms at a repetitive frequency of 3 Hz provided by a DS3 isolated current stimulator (Digitimer Ltd., Welwyn Garden City, Hertfordshire, UK). For all stimuli, the current pulse amplitude was 2 mA, as shown in Figure 3C. Each block was stimulated for 5 s, which included 15 stimulation pulses, with a 1 h interval between each stimulation. Each rat received baseline measurements of ECoG and CBF before photothrombotic ischemia. Thirty minutes after photothrombotic ischemia was induced, each rat underwent four sequential ECoG-LSCI recordings with a 1-h interval between consecutive frames. The 30 s ECoG-LSCI recording included 5 s of peripheral electrical stimulation in each recording frame. Figure 3D shows four continuous ECoG-LSCI recording frames as a representative peripheral electrical stimulation time program.

LSCI data analysis

The speckle images were generated in a LabVIEW environment using an algorithm based on the spatial statistics of the photographed speckle pattern. The spatial laser speckle contrast, K, is given by[40]

$$K\ =\ \frac{\sigma}{\langle I \rangle} \quad \text{(Equation 3)}$$

where σ is the standard deviation and ⟨I⟩ represents the regional mean of the speckle intensity pattern in practice, which was measured in a window of 5 × 5 pixels. Additionally, Fercher and Briers[41] derived the following equation for K based on the relationship between the correlation time (τc) of the backscattered light from the sample and the camera exposure time (T).[42]

$$K\ =\ \sqrt{\frac{\tau c}{2T}\left\{1\ -\ exp\left(\frac{-2T}{\tau c}\right)\right\}} \quad \text{(Equation 4)}$$

Since cortical tissue with quicker blood flow looks blurrier in photographs than tissue with slower or no blood flow, the degree of blurring at each pixel can be measured as a speckle contrast value K, which is associated with relative flow dynamics.[42] The speckle contrast in the time-averaged speckle pattern can also be expressed using Equation 4 as a function of the exposure time (T) and the correlation time $\tau c\ =\ \frac{\lambda}{2\pi V}$, where V is the mean velocity of the scatterers (flow speed) and λ is the optical wavelength of the coherent source.[43] Equation 4 can thus be rewritten as follows.

$$K^2\ =\ \frac{\lambda}{4\pi TV}\left\{1\ -\ exp\ \ exp\left(\frac{-4\pi TV}{\lambda}\right)\right\} \quad \text{(Equation 5)}$$

The LSCI experiments in this study used an optical wavelength of 660 nm, which yielded $\frac{-4\pi TV}{\lambda} < 10^{-7}$ and implied exp $(\frac{-4\pi TV}{\lambda}) \rightarrow 0$. As a result, the flow speed should be expressed as follows.

$$V \propto \frac{1}{TK^2} \quad \text{(Equation 6)}$$

The CBF measured via LSCI is inversely proportional to K^2 in Equation 6. To generate K^2 maps via LSCI, a 5 × 5 pixel window was applied to 10 continuous speckle frames, which were then averaged to reduce noise.[42,44]

The responses to changes in CBF at different time points after photothrombotic ischemia in the blood vessels of the S1FL region, which was calculated as the normalized ratio of CBF ($rCBF_N$), were quantified using the following equation[43]:

$$rCBF_N(T_n) = \frac{R(T_n)}{R(T_b)} \quad \text{(Equation 7)}$$

where $R(T_b)$ is the baseline relative to the average value of resting CBF fluctuations before photothrombotic ischemia and $R(T_n)$ is the average resting CBF fluctuation for the n^{th} time window after photothrombotic ischemia.

Data analysis of the ECoG recordings

SSEPs were induced by electrical stimulation of the forepaw, followed by recording of the SSEP signals before and after photothrombotic ischemia induction. During a 30-s recording, the right SSEPs were low-pass filtered at 150 Hz and high-pass filtered at 250 Hz and then sampled at 10 kHz. MATLAB (MATLAB R2020a, MathWorks, Inc., USA) was used to analyze the SSEPs induced by electrical stimulation of the forepaw. The SSEP amplitude was taken as the average of 15 measurements to generate an average SSEP over a 0.2-ms period for the poststimulus pulse.[20] Changes in the SSEP amplitude were calculated to evaluate changes in evoked potentials during forelimb stimulation before and after the induction of photothrombotic ischemia.

Quantification of the infarct volume

Twenty-four hours after photothrombotic ischemia, the rats in the three groups (n = 13), the sham control (n = 3), photothrombotic ischemia (n = 5) and photothrombotic ischemia+topiramate (n = 5) groups, were sacrificed by overdose of 5% isoflurane (Bowlin Biotech Corp., Taipei, Taiwan) in oxygen to provide excessive anesthesia; then, their brains were removed. Each brain was rinsed with saline and cut into 2 mm coronal sections for 2% TTC (T8877; Sigma–Aldrich Corp., St. Louis, MO, USA) staining at room temperature for 20 min.[45] ImageJ software (National Institutes of Health, Bethesda, MD, USA) was used to analyze the stained brain section images, and the calibrated infarct volume in the sections was identified by the lack of staining. Calibrated infarct volume = [total lesion volume − (nonischemic hemisphere volume – ischemic hemisphere volume)]/ischemic hemisphere volume] × 100%.[46]

Nissl staining

Rats (4 rats per group; total n = 12) were sacrificed using 5% isoflurane. After the rats were sacrificed, their brains were removed, and the brain tissue was soaked in 8% paraformaldehyde solution. The tissues were then embedded in paraffin and cut into 3 mm sections. These paraffin sections were subsequently deparaffinized, rehydrated, washed with PBS, and stained with Nissl for 10 min at 37°C. Then, the sections were washed with distilled water for a few seconds. When the cells could be observed under a microscope and staining was ideal, the sections were dehydrated with graded ethanol, clarified with xylene, and sealed.[47,48]

Western blotting

Additional groups of animals were sacrificed 48 h after photothrombotic ischemia, with 6 rats per group (total n = 18) used for Western blotting. The animals were sacrificed by treatment with an overdose of 5% isoflurane in oxygen to provide excessive anesthesia, after which the brains were removed rapidly. The right cerebral cortex was extracted from each brain, and the brain tissue was separated into the ischemic core, penumbra, and distant cortex and stored at −80°C before use. Tissues were agitated in freshly prepared radioimmunoprecipitation assay (RIPA) lysis buffer containing protease inhibitors, followed by centrifugation at 13,000 r/min for 15 min at 4°C. The protein concentration in each sample was measured using the Thermo Fisher Pierce BCA Protein Assay Kit (Thermo Fisher Scientific, Inc., Waltham, Massachusetts, USA). Twenty microliters of total protein from each sample was subjected to SDS–PAGE (8% or 10%) and transferred to a polyvinylidene fluoride (PVDF) membrane (Millipore, Inc., Burlington, Massachusetts, USA). Skim milk (diluted to 5% in TBS buffer) was then used to block the PVDF membrane at room temperature for 1 h, after which the membrane was incubated at room temperature for 2 h with the following primary antibodies: rabbit anti-NeuN (1:1000, Abcam, Inc., Cambridge, United Kingdom, ab177487), rabbit anti-BDNF (1:1000, Abcam, Inc., Cambridge, United Kingdom, ab108319), rabbit anti-CD68 (ED1) (1:1000, Abcam, Inc., Cambridge, United Kingdom, ab125212), goat anti-Iba-1 (1:1000, Abcam, Inc., Cambridge, United Kingdom, ab5076), goat anti-GFAP (1:500, Santa Cruz Biotechnology, Inc., Dallas, Texas, USA, sc-6170), rabbit anti-BAX (1:2000, Proteintech, USA, 50599-2-Ig), mouse anti-Bcl-2 (1:2000, Proteintech, USA, 68103-1-Ig) or mouse anti-β-actin (1:200, Santa Cruz Biotechnology, Inc., Dallas, Texas, USA, sc-47778). After three washes with 5% milk dissolved in TBS (5 min/wash), the membrane was incubated with homologous HRP-conjugated secondary antibodies (1:10000, Abcam, Inc., Cambridge, United Kingdom) at room temperature for 1 h, washed again with 5% milk dissolved in TBS three times (5 min/wash) and then washed with TBS three times (5 min/wash). The blots were visualized in enhanced chemiluminescence (ECL) solution (Millipore, Inc., Burlington, Massachusetts, USA).

QUANTIFICATION AND STATISTICAL ANALYSIS

The averages of all collected experimental data were calculated, and the results are presented as the means ± standard errors of the means (SEMs). GraphPad Statistics version 8 (GraphPad Software, IL, USA) was used to statistically analyze the data. *t* tests were conducted to analyze the number of CSDs induced by KCl and compare the number of PIDs in the photothrombotic ischemia group and the topiramate

administration group. A value of $p < 0.05$ was considered to indicate a significant difference. Differences in infarct volume between groups were compared using nonparametric paired *t* tests. A probability value of $p < 0.05$ was used as a standard for determining statistical significance. Analysis of variance (ANOVA) was used to evaluate changes in the CBF following photothrombotic ischemia and changes in the SSEP amplitude in different brain areas.[49,50] A *t* test was used to compare the Western blotting data among the control group, photothrombotic ischemia group and photothrombotic ischemia+topiramate group. A value of $p < 0.05$ was considered to indicate a significant difference.